ACS OMEGA

Open Access

http://pubs.acs.org/journal/acsodf

Article

Molecular Recognition of *Moringa oleifera* Active Compounds for Stunted Growth Prevention Using Network Pharmacology and Molecular Modeling Approach

Arwansyah Arwansyah,* Abd Farid Lewa,* Muliani Muliani, Siti Warnasih, Apon Zaenal Mustopa, and Abdur Rahman Arif*

Cite This: *ACS Omega* 2023, 8, 44121−44138

Read Online

ACCESS | Metrics & More | Article Recommendations | Supporting Information

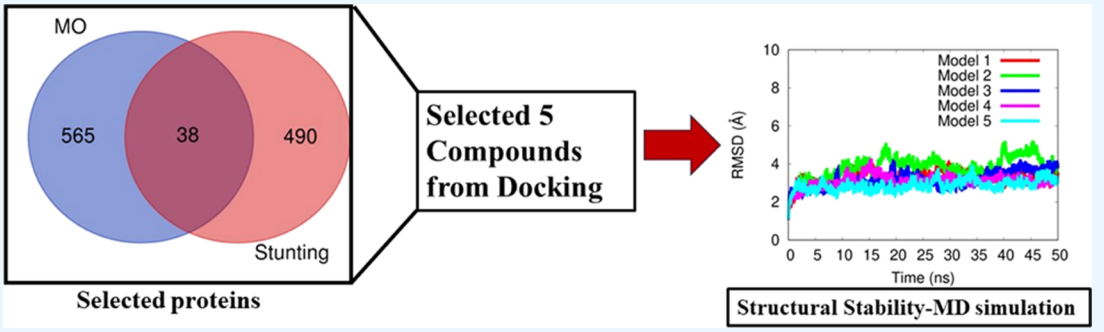

ABSTRACT: In this study, network pharmacology was used to analyze the active compounds of *Moringa oleifera* as food supplements for stunted growth prevention. Thirty-eight important proteins were discovered that may be strongly related to stunting. Those proteins were uploaded to several online tool platforms in order to determine the shared genes' pathways. Six pathways were identified that may be correlated with human growth. Furthermore, ligands for molecular docking analysis were retrieved from the top 5 active substances discovered through experimental investigation. In the meantime, the first-degree rank based on the protein−protein interaction (PPI) topological analysis was utilized to choose albumin protein (ALB) as a receptor. Our docking results showed that every ligand binds to the receptors, indicating that they can bind to the binding site of the ALB protein to form a complex formation. Further, MD simulation was used to verify the stability of the ligand in complex with the protein in the TIP3P water model. Based on the validation parameters, our results suggested that all models achieved a stable phase along the simulation. Additionally, the MM-GBSA method was used to calculate the binding energies of all models. Ligands 2 and 4 have strong binding to the binding pocket of ALB, followed by ligands 3, 5, and 2, suggesting that those ligands could be promising food supplements that can be utilized for the prevention of stunted growth in children.

INTRODUCTION

Stunting is a chronic nutritional condition initiated by a lack of nutrition over the long term, leading to impaired growth in children. In 2017, more than half of the stunting in the world came from Asia (55%), while more than a third (39%) lived in Africa. Of the 83.6 million stunted children under five in Asia, the highest proportion comes from South Asia (58.7%) and the lowest proportion comes from Central Asia (0.9%).[1] Data on the prevalence of stunting under five collected by WHO from 2005−2017 reported that Indonesia is included as the third country with the highest prevalence in the Southeast Asia/Southeast Asia Regional (SEAR) region, in which the average prevalence of stunting under five in Indonesia is 36.4%.[1,2] The government has been attempting to accelerate the reduction of stunting cases by forming a team that can work toward it. The program offers low-income families access to clean water and sanitary facilities, proper dietary intake, regular child health checkups, and other services. However, the number of stunting cases is still high, around 21.6% in 2021, since the WHO recommendation for stunting prevalence must be less than 20%. Furthermore, the Indonesian government wants to reduce the number of cases of stunting to 14% by 2024.[3] Therefore, various efforts are being made to minimize stunting cases because of the significant risks it poses to a child's growth. Consumption of food supplements by utilizing traditional plants is one way to prevent stunting in children.

Received: August 29, 2023
Revised: October 24, 2023
Accepted: October 26, 2023
Published: November 9, 2023

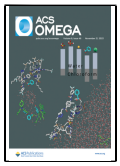

https://doi.org/10.1021/acsomega.3c06379
ACS Omega 2023, 8, 44121−44138

Presently, traditional plants have been popularly exploited for stunted growth prevention since it is thought that traditional plants have medicinal activity to prevent or even treat some diseases. Also, due to their accessibility, low cost, and lesser side effects, medicinal plants are used by around 80% of the people worldwide, especially in developing countries.[4] As a result, there is a significant increase in demand for traditional plants in the healthcare sector in order to avoid or alleviate a variety of illnesses. In Southeast Asia, at least 80% of the medicinal plant species can be found in Indonesia, and 5490 medicinal plants have been reported.[5]

Moringa oleifera is one of the popular plants utilized by people to treat some diseases.[6,7] Pregnant and breastfeeding mothers consume *M. oleifera* leaves to prevent stunting in their children.[8,9] In Central Sulawesi, a province in Indonesia, local people consume *M. oleifera* leaves as a vegetable soup to fulfill their daily nutrition.[10] To understand the pharmacological action of the plant, molecular investigations on the active compounds of *M. oleifera* in binding with the proper protein target related to stunted growth need to be conducted. In experimental analysis, a number of active compounds of *M. oleifera* leaves have been identified, such as quercetin, quinic acid, 2-dimethyl(trimethylsilylmethyl), silyloxymethyltetrahydrofuran, and so on.[11] However, it is difficult to decide which of those active compounds are related to the growth hormone in humans. Therefore, to address this concern, a variety of methods are required to establish the link between these compounds and human growth.

In this study, network pharmacology is implemented to understand the potency of active compounds in *M. oleifera* for preventing stunted growth in children. In this method, some integrated network analyses, such as target gene prediction, interaction between proteins, pathways, and gene ontology (GO) analysis, are employed to recognize the pivotal target protein connected to the growth hormone. Moreover, to gain insights into the molecular mechanism of the active compound of *M. oleifera* at the catalytic site of the protein target, molecular docking is carried out. This method is extensively used to construct a new drug because it can find the orientation pose of a particular small molecule in binding with a receptor.[12−14] To assess the stability of a molecular docked ligand−receptor complex, we perform all-atom molecular dynamics (MD) and estimate validation metrics such as root-mean-square deviation (RMSD), root-mean-square fluctuation (RMSF), radius of gyration (R_g), solvent-accessible surface area (SASA), and hydrogen bonds. Moreover, the thermodynamic quantities of the constructed complex are estimated from the collected trajectories of the MD simulation. A combination of network pharmacology and in silico methods is used not only to provide a better understanding of the molecular interaction between the ligand−receptor complex but also to exhibit substantial implications for the future development of *M. oleifera* compounds to prevent stunted growth.

MATERIALS AND METHODS

Extraction and Elucidation of *M. oleifera* Active Compounds. The *M. oleifera* leaves were retrieved from Palu City, South Sulawesi, Indonesia. To conduct the extraction process, dry powder of the leaves was made and mixed with methanol in the ratio of 1:1 20 (w/w). The extraction process was performed at 45 °C for 20 min with constant stirring using a magnetic stirrer. The resulting extract was filtered and concentrated on a rotary evaporator to obtain a thick methanolic extract.[15] Fourier-transform infrared (FTIR) spectra of methanol extracts from leaves of *M. oleifera* were analyzed using an FTIR spectrophotometer (Shimadzu Corporation) at wavenumbers of 4000−450 cm^{-1}. A mass spectrometer (Xevo G2-S QTof, Waters) and ultraperformance liquid chromatography (UPLC) (LC: ACQUITY UPLC H-Class System, Waters) were used to conduct high-resolution mass spectrometry investigations. This required the use of a C18 column (1.8 m, 2.1 mm × 100 mm, ACQUITY UPLC HSS, Waters) at 25 °C in the room and 50 °C in the column. The mobile phases for the LC analysis were water +5 mM ammonium formic acid (A) and acetonitrile +0.05% formic acid (B). The flow rate for the 23 min slide-moving phase was 0.2 mL/min (step gradient), and the injection volume was 5 L (first filtered through a 0.2 m syringe filter). The mass range of the electrospray ionization (ESI) used for mass spectrometry (MS) analysis was 50−1200 m/z, and the source and desolvation temperatures were 100 and 350 °C, respectively. The collision energy ranged from 4 to 60 eV, and the matching cone and desolvation gas flow rates of 0 and 793 L/h were also utilized. Version 4.1 of the Masslynx software was utilized for instrument control as well as data processing.[16]

Prediction of the Active Compound Target. Several integrative software such as TargetNet,[17] SEA,[18] and SwissTargetPrediction[19] were used by employing different prediction techniques to collect the putative target predictions (genes) of the active compounds of *M. oleifera* relating to stunted growth. The merged genes were inserted into the String database to discover the gene symbol of each prediction target.[20,21] To prevent disorder across the database and platform in the following analysis, all genes were presented in terms of the HUGO Gene Nomenclature Committee (HGNC) gene symbol. The entry with a "*Homo sapiens*" origin was computed in the following analysis. All genes were then combined, and a Venn diagram was made to show where the overlaps occurred. The compound target from the databases was further analyzed using the ClueGo plugin of Cytoscape.[22] The complete protein−protein interactions (PPIs) of within 22 secondary metabolites of *M. oleifera* are shown in Figure S1 of the Supporting Information.

Relation of the Known Protein Target Acting on Stunted Growth. In the GeneCard database (https://www.genecards.org/), the protein targets related to stunted growth were searched by setting the keyword "stunted growth in human".[23] Afterward, all targets were input into the String database to obtain the gene symbol of each target. The repeated targets were removed. Then, a Venn diagram was applied to visualize the overlapped and particular targets.

Network Formation and Validation. The interconnection between active compounds of *M. oleifera* and their potential targets in stunted growth prevention was examined by designing a protein−protein interaction (PPI) network using the STRING database merged with Cytoscape.[24] The protein targets were taken from the predicted genes of three databases and stunted growth targets (predicted genes of the GeneCard database). The construction of the PPI network was visualized by a Venn diagram to identify the similar genes between those targets. The topological identities of each node in the interaction network were then computed, including network centrality (NC), degree, degree centrality (DC), eigenvector centrality (EC), betweenness centrality (BC), closeness centrality (CC), and local average connectivity

https://doi.org/10.1021/acsomega.3c06379
ACS Omega 2023, 8, 44121−44138

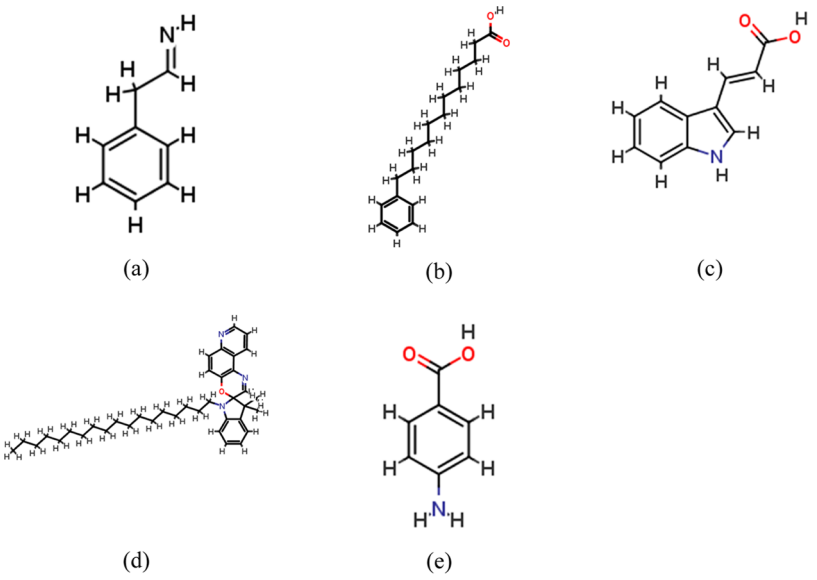

Figure 1. 2D structures of the top five compounds in *M. oleifera* leaves: (a) 2-phenylethanimine, (b) 12-phenyldodecanoic acid, (c) indoleacrylic acid, (d) 3,3-dimethyl-1-octadecyl-1,3-dihydrospiro[indole-2,3′-[1,4] oxazino[3,2-*f*]quinoline], and (e) 4-aminobenzoic acid.

(LAC). The nodes equivalent to the targets with higher ranks were reflected to have a crucial role within the PPI network. Besides, several databases, i.e., MetaScape,[25] WebGestalt,[26] and ConsensusPathDB,[27] were employed to comprehend the biological function inside the created network, GO/KEGG analysis for the target network, the compound-target network, and the target-pathway network. To display the GO/KEGG function, the GO Enrichment plot constructed using ImageGP (http://www.ehbio.com/ImageGP/) was used. The database, software, and online tool used in the current investigation are provided in Table S2.

Docking Study. To obtain the binding site of the active compounds of *M. oleifera* (ligands) into the pivotal site of the protein target (receptor), molecular docking was carried out using AutoDock Vina program packages created by Trott and co-workers.[28] At present, the top five compounds based on % value were retrieved for further analysis. The chemical structures of those compounds retrieved using the PubChem database (https://pubchem.ncbi.nlm.nih.gov/)[29] are presented in Figure 1. Those ligands are saved for the SDF extension. Then, Open Babel 2.4.1 program packages were employed to convert SDF files to the PDBQT format.[30] The charges of the ligands were automatically inserted by the program default. In receptor preparation, the tertiary structures of the protein target are downloaded from the RSCB database with PDB ID: 6QIO. The tertiary structure of the receptor is presented in Figure 2. The polar hydrogen and Kollman's united atom charges are inserted into the receptor. Afterward, the protein target is saved in the PDBQT format.

In molecular docking simulations, the grid box parameters need to be assigned with enough space for positional and rotational position of the selected ligands into the catalytic site of the protein targets. The parameters grid box size (--size_x 30, -size_*y* 30, -size_*z* 30), grid box center (-center x 17.447, -center_*y*, −23.897, -center_*z* −33.975), and spacing point (1 Å) were set for all protein−ligand systems. The box size was identified at the crucial site of the receptor.[31] The exhaustiveness is computed at 100. Other parameters are set as the default values of AutoDock Vina. The Broyden−Fletcher−Goldfarb−Shanno (BFGS) algorithm is employed as

Figure 2. 3D structures of the selected protein target (human serum albumin) obtained from network pharmacology analysis. The red and green colors correspond to the α helix and coil structures.

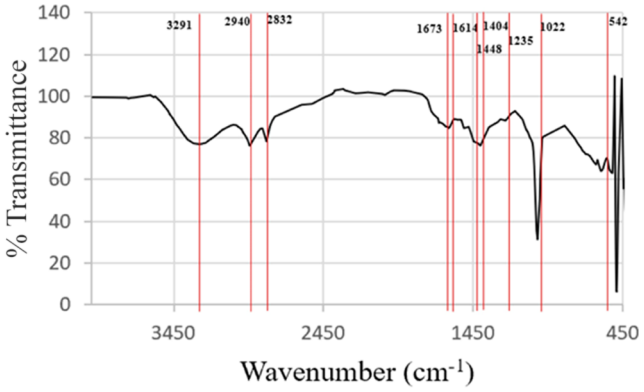

Figure 3. FTIR spectrum of *M. oleifera* leaf extract using a methanol solvent.

a searching parameter to find the catalytic site of the selected compound in the site of the target proteins. All docking parameters are computed by using AutoDock Tools 1.5.6 developed by Morris and co-workers.[32] The docking procedure was carried out according to similar protocols presented in our previous studies.[33−35]

Molecular Dynamics Simulation. To assess the stability of the complex produced via molecular docking, all-atom

https://doi.org/10.1021/acsomega.3c06379
ACS Omega 2023, 8, 44121−44138

Table 1. List of FTIR Spectra Analysis of *M. oleifera* Leaf Extract

functional groups		wavenumber		vibration
		results	literature	
O−H	alcohol	3291	3570−3200	stretch
C−H	alkane	2940, 2832	2935−2915/2865−2845	stretch
C═C	alkene	1673	1680−1620	stretch
N−H	secondary amine	1614	1650−1550	bend
C−H	alkane	1448, 1404	1470−1430/1380−1370	bend
aril −O−H	aromatic ether	1235	1270−1230	stretch
C−N	primary amine	1022	1090−1020	stretch
C−S	sulfide	542	570−705	stretch

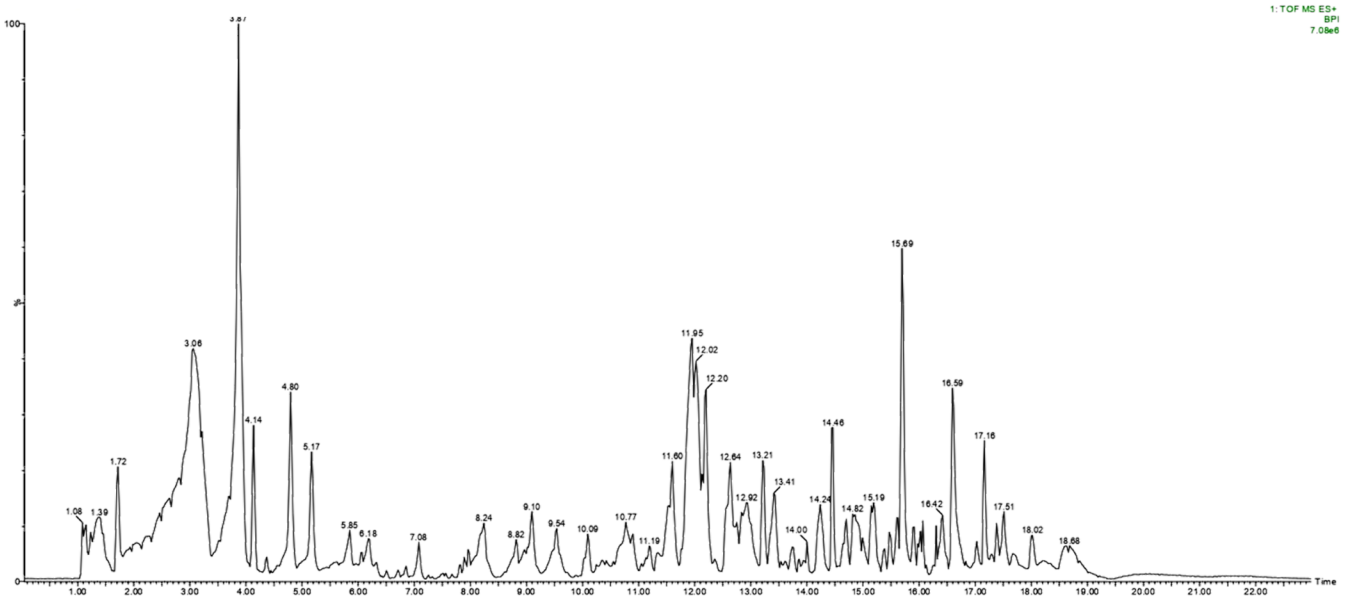

Figure 4. Chromatogram of LC-MS of *M. oleifera* methanolic extracts.

molecular dynamics simulation was performed on the receptor−ligand complex using Amber20 software packages.[36] TIP3P solvent models[37] were incorporated into the system's cubic box size. For the purpose of neutralizing the system, the counterions Na+ have been added. The ligand and receptor force field characteristics were generated using the generic AMBER force field (GAFF)[38] and the AMBER force field (ff14SB),[39] respectively. Particle mesh Ewald (PME)[40] algorithms were used to set the electrostatic interactions, while SHAKE[41] methods were used to confine the distance of the hydrogen atom. The switching cutoff distance was set to 10 Å. For all simulations, a time step of 2 fs was used. The MD simulation began with an energy minimization of the system. The temperature was then steadily increased from 0 to 300 K by performing an NVT-constant for 500 ps. Using the Langevin thermostat[42] and the isotropic position scaling technique, the system temperature as well as pressure were regulated at 300 K and 1 atm, respectively. The system was equilibrated with the NPT ensemble for 50 ns before recording the trajectory every 5000 steps (10 ps). The CPPTRAJ tool was used to examine the MD simulation trajectories.[43] The complex's root-mean-square deviation (RMSD) was calculated to assess the ligands' stability in interacting with the receptor using the following equation:

$$\mathrm{RMSD}\ (t_1) = \left[\frac{1}{M} + \sum_{i=1}^{N} m_i \left\| r_i(t_1) - r_{\mathrm{ref},i} \right\|^2\right]^{1/2} \quad (1)$$

where N is the total number of atoms in the model complex, m_i is the mass of atom i, M is the total mass of all atoms, r_i is the position of atom i at time t, and $r_{\mathrm{ref},i}$ is the positions of the i-th atom in the X-ray structure. The contribution of energy to the ligand in binding with the receptor was calculated using the molecular mechanics-generalized Born surface area (MM-GBSA) method developed by Miller and colleagues.[44] The following equation was used to compute the binding energy from the MD simulation trajectory

$$\Delta G_{\mathrm{binding}} = -RT \ln Ki = G_{\mathrm{complex}} - (G_{\mathrm{receptor}} + G_{\mathrm{ligand}}) \quad (2)$$

The contribution energies were estimated as follows

$$G = -RT \ln Ki = E_{\mathrm{vdw}} + E_{\mathrm{ele}} + E_{\mathrm{GB}} + E_{\mathrm{SA}} \quad (3)$$

where E_{GB}, E_{SA}, E_{vdw}, and E_{ele} are the general Born solvation, surface area, van der Waals, and electrostatic energies, respectively.

RESULTS

Experimental Analysis of *M. oleifera* Active Compounds. The FTIR spectrum of *M. oleifera* leaf extract using methanol solvent is shown in Figure 3. Meanwhile, the

https://doi.org/10.1021/acsomega.3c06379
ACS Omega 2023, 8, 44121−44138

Table 2. Phytocomponents of *M. oleifera* Leaves Obtained from the Methanol Extract Using LC-MS

no	mass spectrum	formula	compound name	%area
1	120.0801	C_8H_9N	2-phenylethanimine	18.73
2	277.2154	$C_{18}H_{29}O_2$	12-phenyldodecanoic acid	12.04
3	188.0701	$C_{11}H_9NO_2$	indoleacrylic acid	11.92
4	568.4278	$C_{38}H_{54}N_3O$	3.3-dimethyl-1-octadecyl-1.3-dihydrospiro[indole-2.3′-[1.4]oxazino[3.2-*f*]quinoline]	4.19
5	138. 0549	$C_7H_7NO_2$	4-aminobenzoic acid/1-(2-nitrovinyl)-1.3-cyclopentadiene	3.46
6	303.0498	$C_{15}H_{11}O_7$	quercetin	2.78
7	465.1033	$C_{21}H_{21}O_{12}$	hyperoside/2-(3.4-dihydroxyphenyl)-5.7-dihydroxy-4-oxo-4*H*-chromen-3-yl *β*-D-galactopyranoside	2.78
8	433.1133	$C_{21}H_{21}O_{10}$	5-hydroxy-3-(4-hydroxyphenyl)-4-oxo-4*H*-chromen-7-yl hexopyranoside	2.78
9	279.2307	$C_{18}H_{31}O_2$	*α*-linolenic acid	2.69
10	275.1997	$C_{18}H_{27}O_2$	nandrolone/(17*β*)-17-Hydroxyestr-4-en-3-on	2.5
11	293.2105	$C_{18}H_{29}O_3$	12-oxo phytodienoic acid	2.5
12	315.1919	$C_{16}H_{23}N_6O$	*N*-(4-methoxyphenyl)-6-(1-piperidinylmethyl)-1.3.5-triazine-2.4-diamine	2.5
13	695.4037	$C_{38}H_{55}N_4O_8$	1.4-phenylene (2*S*.3*R*.2′*S*.3′*R*)bis[3-{[(2.2-dimethylpropanoyl)oxy]methyl}-2-ethyl-4-(1-methyl-1*H*-imidazol-5-yl)butanoate]	2.48
14	351.2131	$C_{20}H_{31}O_5$	(−)-andrographolide	2.45
15	333.2034	$C_{13}H_{29}N_6O_2S$	2-methyl-2-propanyl [5-({[2-(*N*-methylcarbamimidoyl)hydrazino]carbonothioyl}amino)pentyl]carbamate	2.41
16	275.2003	$C_{15}H_{31}O_2S$	3-(dodecylthio)propanoic acid	2.41
17	277.2158	$C_{18}H_{29}O_2$	12-phenyldodecanoic acid	2.15
18	317.2081	$C_{20}H_{29}O_3$	etienic acid	2.15
19	445.3682	$C_{29}H_{49}O_3$	cholesteryl methyl carbonate	2.13
20	181.1221	$C_{11}H_{17}O_2$	3-BHA/4-methoxy-2-(2-methyl-2-propanyl)phenol	2.08
21	778.5365	$C_{41}H_{72}N_5O_9$	kohamamide C/(3*S*.6*S*.9*S*.13*S*.16*S*.19*S*.24a*S*)-19-[(2*S*)-2-butanyl]-3-isobutyl-13.16-diisopropyl-6.10.10.15-tetramethyl-9-pentyldodecahydro-1*H*.9*H*-pyrrolo[2.1-*i*][1.13.4.7.10.16.19]dioxapentaazacyclodocosine-1.4.7.11.14.17. 20(10*H*.19*H*)-heptone	2.08
22	413.2652	$C_{21}H_{37}N_2O_6$	ethyl (3*R*.4*R*.5*S*)-4-acetamido-5-({[(2-methyl-2-propanyl)oxy]carbonyl}amino)-3-(3-pentanyloxy)-1-cyclohexene-1-carboxylate	2.04
23	803.5421	$C_{45}H_{75}N_2O_{10}$	(1*R*.9*S*.12*S*.13*R*.17*R*.18*E*.21*S*.23*S*.24*R*.25*S*.27*R*)-12-{(1*E*)-1-[(1*R*.3*R*.4*S*)-4-(dimethylamino)-3-methoxycyclohexyl]-1-propen-2-yl}-17-ethyl-1-hydroxy-23.25-dimethoxy-13.19.21.27-tetramethyl-11.28-dioxa-4-azatri cyclo[22.3.1.$0^{4.9}$]octacos-18-ene-2.3.10.16-tetrone	2.04
24	287.0547	$C_{15}H_{11}O_6$	luteolin/3′ 4′ 5 7-tetrahydroxyflavone	2
25	449.1081	$C_{21}H_{21}O_{11}$	quercitrin/3.3′.4′.5.7-pentahydroxyflavone 3-rhamnoside	2
26	179.1063	$C_{11}H_{15}O_2$	2-isopropyl-5-methylbenzoic acid	2
27	565.4026	$C_{40}H_{53}O_2$	canthaxanthin	1.88
28	583.4131	$C_{40}H_{55}O_3$	(3*R*.3′*S*.5′*R*.6′*S*)-7.8-didehydro-5′.6′-dihydro-5′.6′-epoxy-*β*.*β*-carotene-3.3′-diol	1.88
29	107.0486	C_7H_6O	3-ethynyl-4-methylfuran/2.4-cyclohexadien-1-ylidenemethanone	1.65
30	197.1161	$C_{11}H_{17}O_3$	1-carboxy-3-hydroxyadamantane	1.59
31	264.0856	$C_{14}H_{10}N_5O$	2-(2-furyl)-7-(2-pyridinyl)[1.2.4]triazolo[1.5-*a*]pyrimidine	1.59
32	797.5171	$C_{42}H_{73}N_2O_{12}$	(3*R*.4*S*.5*S*.6*R*.7*S*.9*R*.10*S*.11*R*.12*R*.13*S*)-10-(dimethylamino)-6-{[(2*S*.3*R*.4*S*.6*R*)-4-(dimethylamino)-3-hydroxy-6-methyltetrahydro-2*H*-pyran-2-yl]oxy}-14-ethyl-7.12.13-trihydroxy-3.5.7.9.11.13-hexamethyl-2-oxooxa cyclotetradecan-4-yl 2-(methoxymethoxy)-3-phenylpropanoate	1.38
33	163.111	$C_{11}H_{15}O$	1-phenyl-1-pentanon/valerophenone	1.22
34	240.2317	$C_{15}H_{30}NO$	*N*-dodecylacrylamide	0.76
35	450.2271	$C_{27}H_{32}NO_5$	2-methyl-2-propanyl [2.2-dimethyl-5-(6-phenoxy-2-naphthyl)-1.3-dioxan-5-yl]carbamate	0.48

identification of functional groups in the sample is listed in Table 1. The broad spectrum at 3450 cm^{-1} shows the absorption of the hydroxyl group.[45] C−H stretching absorption was found at 2940 and 2832 cm^{-1}.[46] The peaks around 1673 and 1614 cm^{-1} correspond to the stretching absorption of C═C and bending of N−H groups.[47,48] The peaks at 1448 and 1404 cm^{-1} indicated C−H bending of alkanes.[49] The aromatic ether group of aryl O−H is shown at 1235 cm^{-1}.[50] In addition, the presence of C−N (primary amine) and C−S (sulfide) groups was detected at 1090−1020 and 705−570 cm^{-1}.

Figure 4 shows the liquid chromatography−mass spectrometry (LC−MS) data with 35 chromatogram peaks indicating the number of compounds present in *M. oleifera* extract. Five main compounds were identified with concentrations above 3% based on the percentage area data from LC-MS analysis. These compounds include 2-phenylethanimine (18.73%), 2-phenyldodecanoic acid (12.04%), indoleacrylic acid (11.92%), 3,3-dimethyl-1-octadecyl-1,3-dihydrospiro[indole-2,3′-[1,4]-oxazino[3,2-*f*]quinoline] (4.19%), and 4-aminobenzoic acid (3.46%). The distribution of major compounds with high concentrations in plant extracts is estimated to play a significant role in biological activity.[15]

Particular Target Prediction of Active Compounds in *M. oleifera*. The secondary metabolites of *M. oleifera* leaves were obtained from the experimental analysis as shown in Table 2. Additionally, for the purpose of predicting the relation between the *M. oleifera* active compounds and stunted growth prevention, the SMILE identities of each active molecule deposited in the PubChem database (https://pubchem.ncbi.nlm.nih.gov/)[29] were retrieved for further analysis. 22 of 35 active compounds were identified in the PubChem database. Hence, at present, only those 22 compounds were retrieved and used for further analysis. The PubChem ID and SMILE identities of those compounds are provided in Table S1 of the Supporting Information. To determine the targets of the *M.*

https://doi.org/10.1021/acsomega.3c06379
ACS Omega 2023, 8, 44121−44138

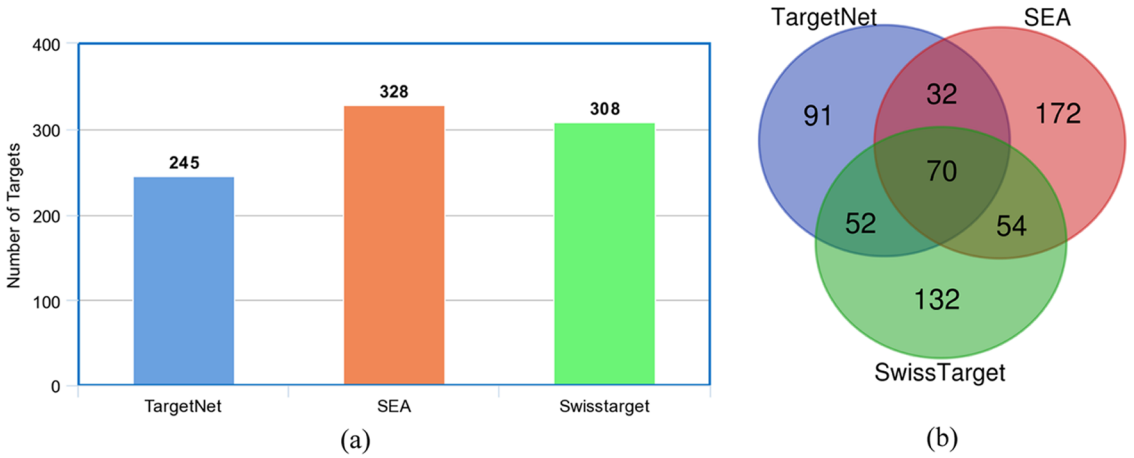

Figure 5. Examination of the predicted genes for *M. oleifera*'s 22 active compounds from three databases. (a) Predicted gene numbers from TargetNet (blue), SEA (orange), and SwissTarget (green); (b) Venn diagram illustrating the overlapping and particular genes predicted from those three databases.

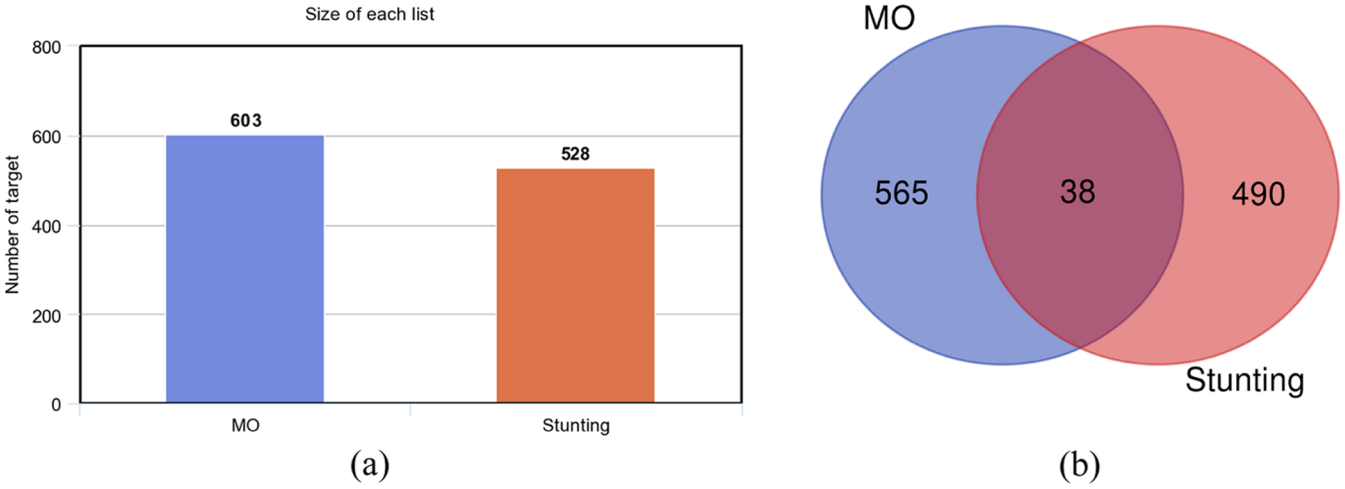

Figure 6. Examination of the predicted compound-target genes for *M. oleifera* (MO) compounds as well as stunted growth. (a) Predicted gene numbers from each data set; (b) Venn diagram showing the number of overlapped and particular genes from both MO substances and stunting.

oleifera compound, several databases including SwissTarget, SEA, and TargetNet online platforms were employed. As demonstrated in Figure 5(a), we discovered numerous targets from TargetNet (245 targets), SEA (328 targets), and SwissTarget (308 targets). Upon eliminating the redundant targets, the overlapped genes are found, as shown in Figure 5(b). 138 genes were found in two databases, and 70 were distributed by three online platforms. 208 specific genes were identified in all databases after the overlapped genes were removed. In total, 603 genes were obtained and chosen as the favorable target for the active compounds to prevent stunted growth. Then, the 603 genes were input to the ClueGO tool to provide their network connections (Figure S1).

Identification of Approved Therapeutic Targets in Stunted Growth. The GeneCard database was used to locate the approved target that affects stunting, as well as to determine the gene similarity between those existing therapeutic targets and the target prediction. Figure 6(a) shows the obtained 565 gene targets from the previous three platforms (*M. oleifera* in the blue chart), while 490 genes of the approved therapeutic target are identified from GeneCard (stunted growth in the orange chart). As a result, 38 genes were found relating *M. oleifera* to stunted growth, as visualized by the Venn diagram (Figure 6(b)).

Network Construction and Topological Analysis. The STRING online tool and Cytoscape software package were implemented to build a protein−protein interaction (PPI) network on the 38 genes and assess their networks using the "default parameter in confidence: 0.40" (Figure 7). To eliminate confusion between databases and platforms, the HUGO Gene Nomenclature Committee (HGNC) gene symbol was used for all genes. The PPI topological evaluation was then computed by utilizing the CytoNCA program. Table 3 shows the topological analysis results and parameters. We found that human serum albumin (ALB), (Interleukin 6) IL6, and (estimated glomerular filtration rate) EGFR proteins were the top three-degree rank based on the topological network analysis, indicating they may have a strong connection with stunted growth. Additional parameters, listed in Table 3, are given in columns 3−9. The results implied that no discernible distinction was seen when the gene target was ranked using other criteria.

Integrated Target Pathways and GO Analysis. The MetaScape server was employed on 38 shared targets to verify several pathways in the "*M. oleifera* and Stunted growth"

https://doi.org/10.1021/acsomega.3c06379
ACS Omega 2023, 8, 44121−44138

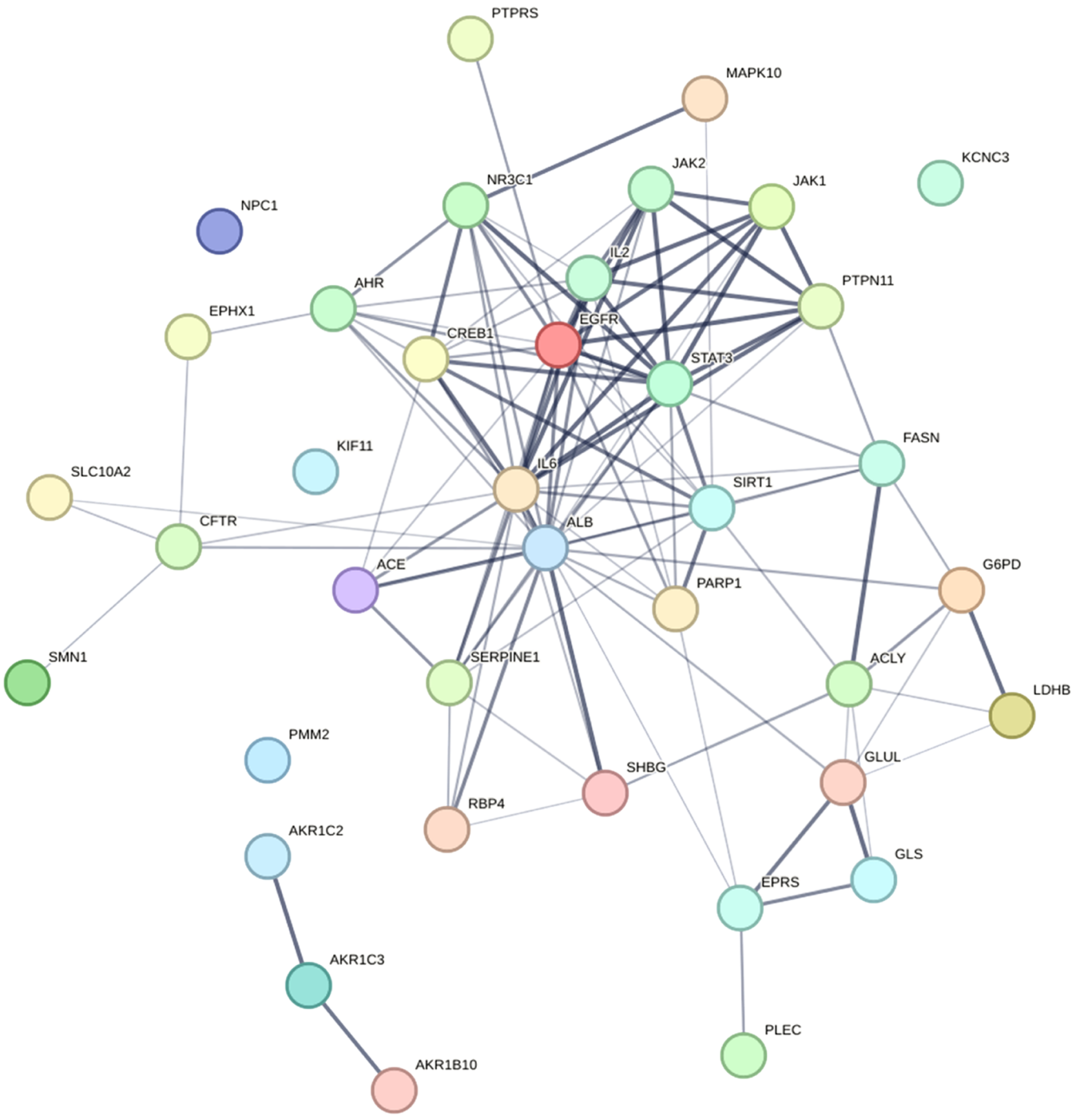

Figure 7. Protein−protein interaction (PPI) network of the 38 target genes is visualized in the 3D form. The network was built using the STRING Web server with the network threshold of 0.4.

network. The compound-target network was shown by the integrated pathways displayed and the heatmap of GO analysis displayed in Figure 8. The pathway of "regulation of growth" was identified and connected to stunted growth. This finding implied that those 38 shared proteins have a strong correlation with human growth. Further, 38 genes connecting *M. oleifera* and stunted growth were inserted into the webGestalt database for GO enrichment analysis. Figure 9 shows three components such as cellular component (CC), biological process (BP), and molecular function (MF) in all genes. In the biological process (Figure 9(a)), "developmental process", "growth", and cell proliferation correlated with human growth. Meanwhile, the findings in cellular components and molecular functions could also be connected to cell growth, as shown in Figure 9(b),9(c), respectively.

Integrative Network Analysis and Target Selection. To decide the pathways of the obtained protein targets, 38 genes were submitted to the ConsensusPathDB-human platform. Ten pathways were found as provided in Figure 10. "Signaling of hepatocyte growth factor receptor", "Disease of signal transduction by growth factor receptors and second messengers", "Growth hormone receptor signaling", "Growth hormone signaling", "Growth hormone synthesis, secretion, and action", and "Mammary gland development pathway" were

https://doi.org/10.1021/acsomega.3c06379
ACS Omega 2023, 8, 44121−44138

Table 3. Topological Network Evaluation of the PPI Network Based on the 38 Target Genes Shared by *M. oleifera* Active Substances and Stunted Growth[a]

no.	gene symbol	degree	subgragh	eigenvector	LAC	betweenness	closeness	network
1	ALB	21	0.36	3.01	6.57	255.70	0.12	18.04
2	IL6	19	0.35	2.97	7.05	176.60	0.12	16.34
3	EGFR	16	0.33	2.90	7.50	82.92	0.12	13.63
4	STAT3	13	0.30	2.80	7.85	14.35	0.12	11.52
5	SIRT1	11	0.26	2.71	7.45	6.91	0.12	9.91
6	IL2	10	0.25	2.66	7.00	5.65	0.12	8.58
7	CREB1	12	0.24	2.76	5.50	67.84	0.12	8.72
8	NR3C1	9	0.22	2.60	6.00	23.42	0.12	7.73
9	JAK2	8	0.21	2.53	6.50	0.67	0.11	7.57
10	PTPN11	8	0.20	2.53	6.00	2.35	0.11	7.07
11	AHR	8	0.20	2.53	5.25	36.39	0.11	6.00
12	JAK1	7	0.19	2.45	6.00	0.00	0.11	7.00
13	SERPINE1	8	0.18	2.53	4.75	7.57	0.11	6.55
14	PARP1	7	0.18	2.45	4.29	16.05	0.11	5.08
15	ACE	6	0.16	2.35	4.67	0.33	0.11	5.60
16	FASN	7	0.15	2.45	3.43	19.62	0.11	4.17
17	SHBG	5	0.10	2.23	2.40	9.68	0.11	3.25
18	RBP4	4	0.09	2.09	3.00	0.00	0.11	4.00
19	CFTR	5	0.07	2.23	0.80	77.61	0.11	1.75
20	ACLY	7	0.06	2.45	1.71	33.22	0.11	3.35
21	G6PD	5	0.06	2.23	2.40	20.27	0.11	3.50
22	EPRS	5	0.06	2.23	0.80	78.55	0.11	1.25
23	GLUL	6	0.05	2.35	2.00	47.94	0.11	3.80
24	MAPK10	2	0.04	1.65	1.00	0.00	0.11	2.00
25	SLC10A2	2	0.04	1.65	1.00	0.00	0.11	2.00
26	PTPRS	1	0.03	1.31	0.00	0.00	0.11	0.00
27	EPHX1	2	0.03	1.65	0.00	1.33	0.11	0.00
28	LDHB	3	0.02	1.90	2.00	0.00	0.11	3.00
29	GLS	3	0.02	1.90	1.33	2.00	0.11	2.00
30	SMN1	1	0.01	1.31	0.00	0.00	0.10	0.00
31	PLEC	1	0.01	1.31	0.00	0.00	0.10	0.00
32	AKR1C3	2	0.00	1.65	0.00	2.00	0.03	0.00
33	AKR1C2	1	0.00	1.31	0.00	0.00	0.03	0.00
34	AKR1B10	1	0.00	1.31	0.00	0.00	0.03	0.00
35	NPC1	0	0.00	0.81	0.00	0.00	0.03	0.00
36	PMM2	0	0.00	0.81	0.00	0.00	0.03	0.00
37	KIF11	0	0.00	0.81	0.00	0.00	0.03	0.00
38	KCNC3	0	0.00	0.81	0.00	0.00	0.03	0.00

[a]The degree value was used to sort the given data.

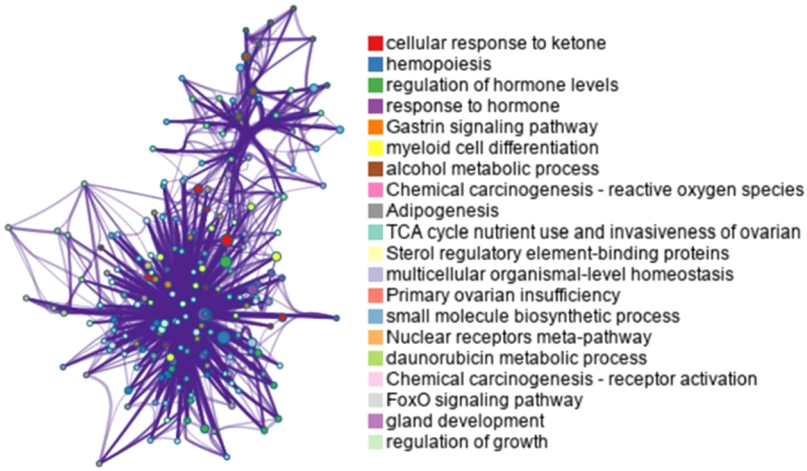

Figure 8. Integrated pathways of 38 protein targets utilizing the Metascape tool.

https://doi.org/10.1021/acsomega.3c06379
ACS Omega 2023, 8, 44121−44138

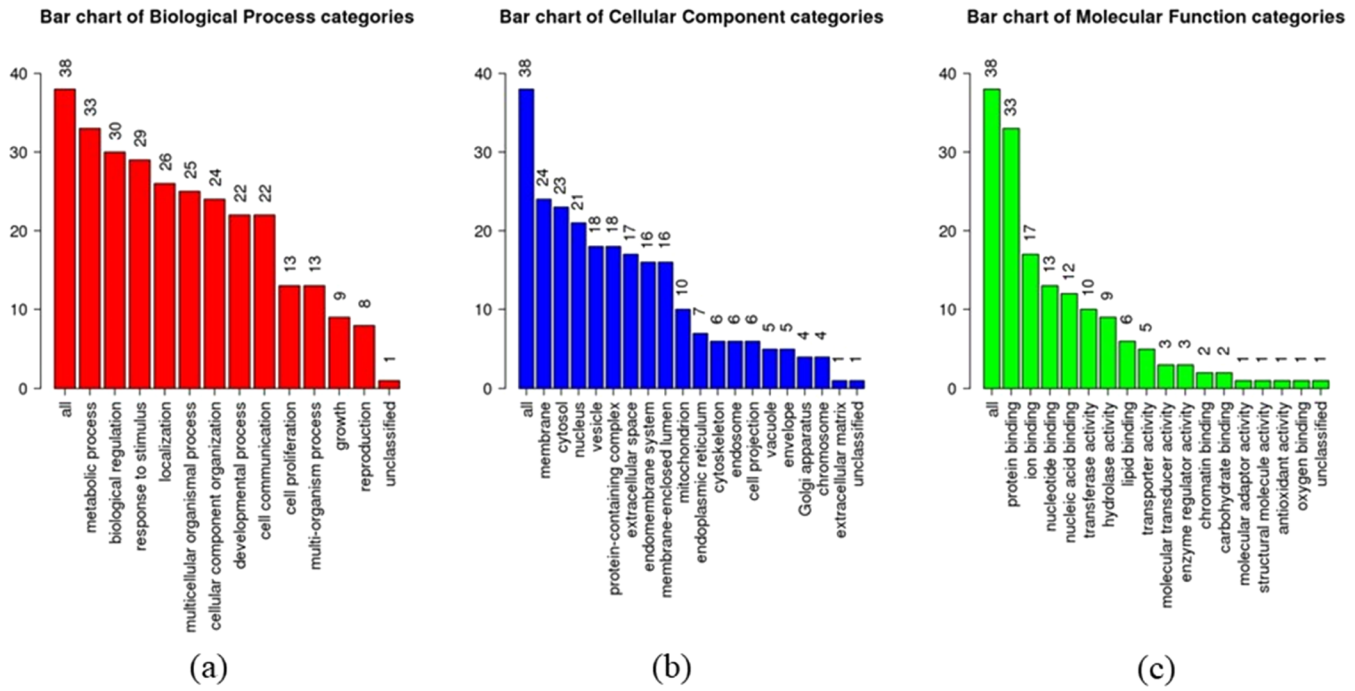

Figure 9. GO analysis of MO chemical target−gene interactions to identify the correlation of (a) biological processes (BPs), (b) cellular components (CCs), and (c) molecular function (MF). The variety of genes is highlighted by the vertical bar graph.

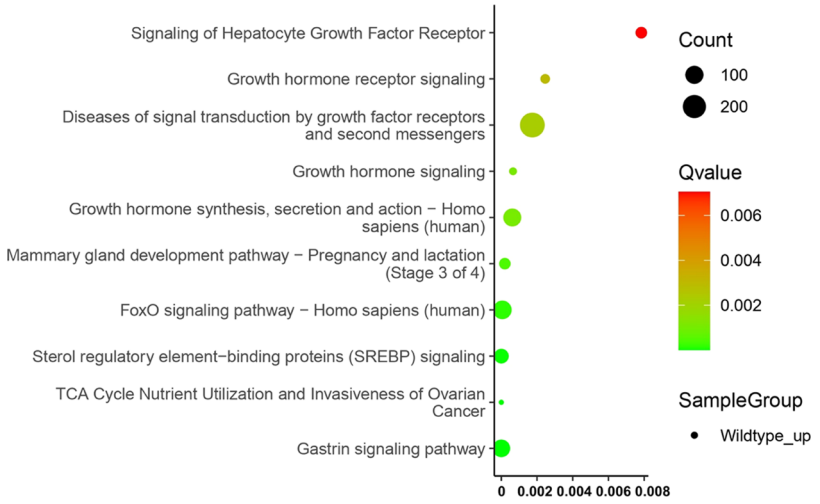

Figure 10. ConsensusPathDB-human library was used to visualize 10 pathways involving 38 genes. The bubble graph displays significant pathways.

found and could be correlated with human growth. Thus, investigation of this pathway is crucial to understanding the human growth mechanism. At present, "Growth hormone synthesis, secretion, and action" pathways are computed in the KEGG database to show their mechanism, as shown in Figure 11.

Cytoscape software was implemented to exhaustively obtain the intersection of 22 active compounds of *M. oleifera*, 38 shared genes, and 10 pathways as displayed in Figure 12. The correlation provided by a convoluted network involved those compounds and their targets in stunted growth.

Molecular Docking Analysis. In the previous analysis using network pharmacology, 38 shared protein targets correlating to stunted growth were identified. To reduce the length of simulation time and computational cost, we chose only the first-degree rank (human serum albumin (ALB)) based on topological analysis as a receptor for molecular docking. The top 5 active compounds (2-phenylethanimine, 12-phenyldodecanoic acid, indoleacrylic acid, 3,3-dimethyl-1-octadecyl-1,3-dihydrospiro[indole-2,3′-[1,4]oxazino[3,2-*f*]-quinoline], and 4-aminobenzoic acid) based on %Area from the experimental analysis were employed as ligands. Table 4 shows the docked energy score of the top five compounds. The ability of the ligand to attach to the receptor site was evident when the protein−ligand complex showed a negative value. From our docking results, we see that all ligands might bind to the receptors, suggesting that they could make stable complexes. Furthermore, high scores of the binding energy were observed on dihydrospiro[indole-2,3′-[1,4]oxazino[3,2-*f*]quinoline]. Our implication is that when pregnant women/nursing mothers consume *M. oleifera* leaves, the compound 3,3-dimethyl-1-octadecyl-1,3-dihydrospiro[indole-2,3′-[1,4]-

https://doi.org/10.1021/acsomega.3c06379
ACS Omega 2023, 8, 44121−44138

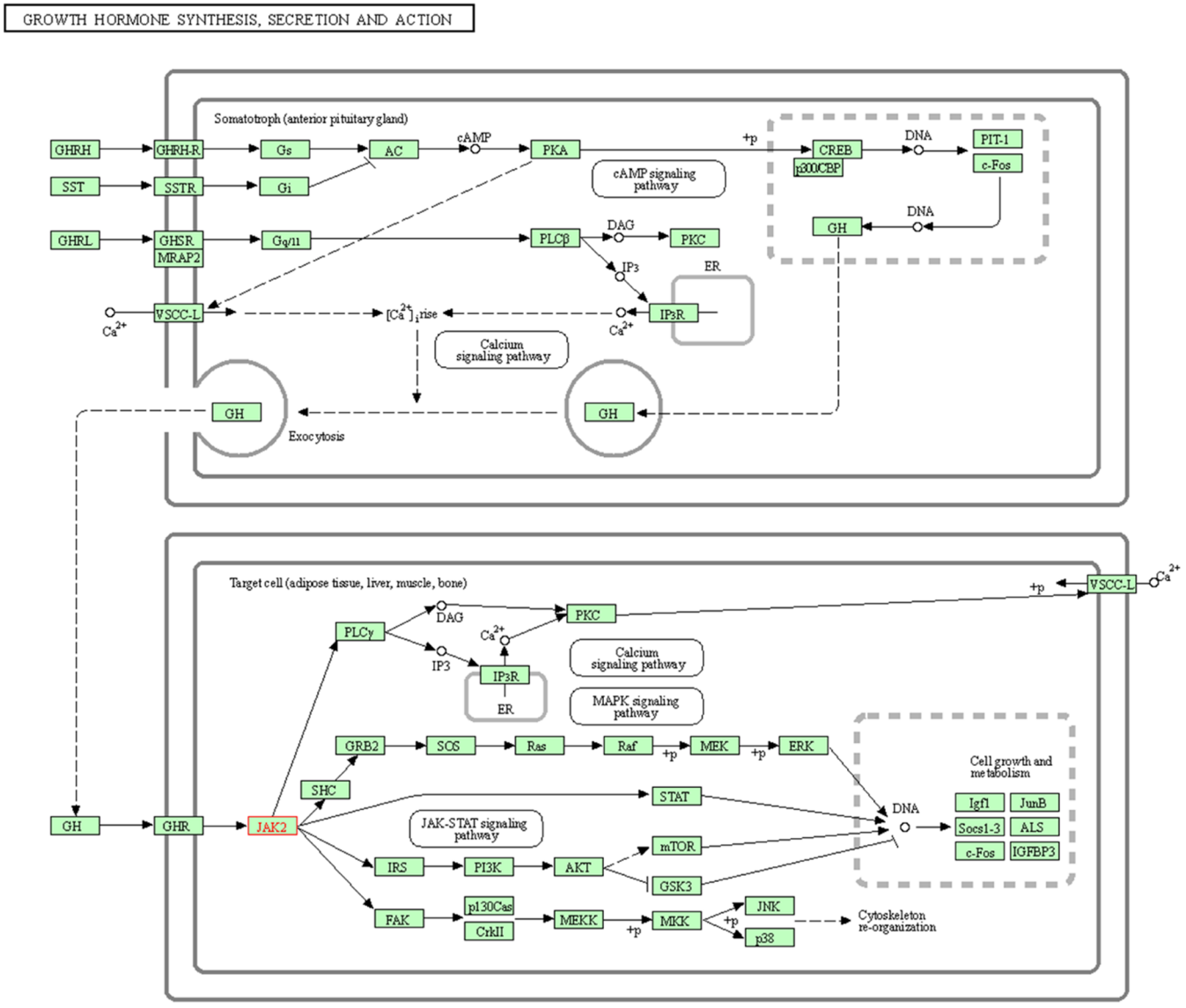

Figure 11. Comprehensive analysis of growth hormone synthesis, secretion, and action pathway in human cells (https://www.kegg.jp/pathway/map04935).

oxazino[3,2-*f*]quinoline] will exhibit a stronger binding affinity with the human serum albumin (ALB) compared to indoleacrylic acid, 12-phenyldodecanoic acid, 4-aminobenzoic acid, and 2-phenylethanimine.

The selected ligands in complex with the main target protein are presented in Figures 13 and 14. These figures show that hydrogen bonds and hydrophobic interactions play a role in the binding of the ligands with the ALB site. The details of hydrogen bonds for all models are listed in Table 5. 2-Phenylethanimine participated in hydrogen bonding with the residue LEU481 of ALB. The residues ARG484 and ARG485 contributed to the hydrogen bonding with 12-phenyldodecanoic acid. For indoleacrylic acid, the hydrogen bond was formed between the side chain of the ligand and one residue ASP451 of ALB. Meanwhile, a hydrogen-bond interaction was noted between 3,3-dimethyl-1-octadecyl-1,3-dihydrospiro-[indole-2,3′-[1,4]oxazino[3,2-*f*]quinoline] and the residue HIS146. For 4-aminobenzoic acid, a hydrogen bond was found with the residue SER202.

On the other hand, hydrophobic interactions of the ligands in complex with ALB have been identified and are summarized in Table 6. 2-Phenylethanimine contributed to hydrophobic interactions with residues LEU198, TRP214, VAL344, LEU347, LEU481, and VAL482. For 12-phenyldodecanoic acid, eight residues are involved in hydrophobic interactions, such as those of LYS195, LEU198, TRP214, VAL343, VAL344, SER454, VAL455, and LEU481. The hydrophobic interactions of indole(acrylic acid) are identified at the residues of LYS195, LEU198, and ASP451. In 3,3-dimethyl-1-octadecyl-1,3-dihydrospiro[indole-2,3′-[1,4]oxazino[3,2-*f*]-quinoline], hydrophobic interactions are observed with residues PRO110, LYS194, LYS432, LYS436, VAL455, and VAL456. The residues LEU198, TRP214, LEU347, and LEU481 of ALB make hydrogen bonds with 4-aminobenzoic acid.

In experimental analysis, the crucial site of ALB was investigated at residues ASN391, TYR411, LEU430, VAL433, APS451, LEU453, SER454, LEU455, LEU481, LEU482, and SER489, suggesting that a ligand that can bind

https://doi.org/10.1021/acsomega.3c06379
ACS Omega 2023, 8, 44121−44138

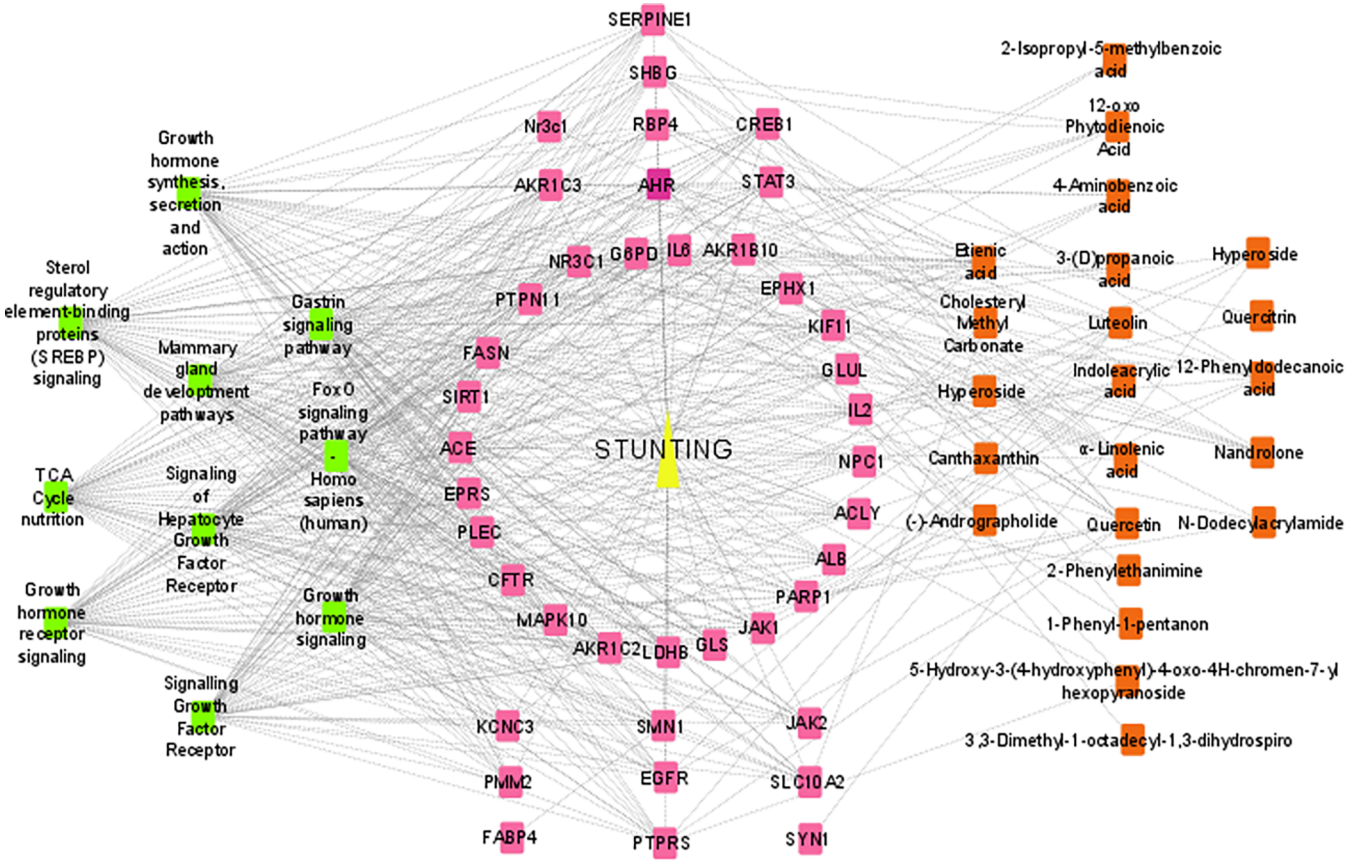

Figure 12. Comprehensive representation of the generated network *of M. oleifera* and stunted growth. The stunting is denoted as yellow, and target genes are presented in pink. The pathways and the active compounds are denoted in green and orange colors, respectively. All edges are presented as black lines.

Table 4. Docking Results of the Top Five Ligands and the Selected Targets (kcal/mol)

no.	compound	binding energy (kcal/mol)
1	2-phenylethanimine	−6.1
2	12-phenyldodecanoic acid	−6.6
3	indoleacrylic acid	−7.4
4	3,3-dimethyl-1-octadecyl-1,3-dihydrospiro[indole-2,3′-[1,4]oxazino[3,2-*f*]quinoline]	−7.9
5	4-aminobenzoic acid	−6.3

with these residues or occupied these residues' regions is predicted to have the ability to increase the ALB activity, facilitating its molecular function. Our docking result shows that all ligands were bound to those sites of ALB via hydrogen bonds and hydrophobic interactions, indicating that the ligands might serve as potential components to increase ALB activity. Thus, they may be used as food supplements to prevent stunted growth.

Molecular Dynamics Analysis. To verify the stability of the ligand−protein complex in a water solvent, MD simulation was carried out. The number of counterions, box size, and water molecules of those five complexes are summarized in Table 7. The complete protocols for MD simulation for the five models have been provided in the subsection Molecular Dynamics Simulation.

A number of validation metrics, such as radius of gyration (R_g), root-mean-square deviation (RMSD), solvent-accessible surface area (SASA), root-mean-square fluctuation (RMSF), and hydrogen bond, were examined to confirm the stability of the complexes obtained from molecular docking. Figure 15(a) shows the RMSD value as a function of the evolution time. In this figure, all models involved small fluctuations at the initial simulation, around 0−5 ns. Then, all complexes reached equilibrium states after 6 ns, although complex 2 is in a small fluctuation at 40−45 ns. Despite the fact that certain fluctuation points were seen for all of the models, this result showed that our models remained stable throughout the simulation. A slight fluctuation during MD simulation is possible since the amino acid residues or ligand molecules require structural redisposition at the ligand−protein contact via electrostatic and van der Waals interactions and even water molecule connections. Figure 15(b) presents the RMSF profile corresponding to the flexibility of the amino acid. The graph trends showed that all models have a tendency to be more flexible in nature, indicating that the interaction between the ligand and the protein may be easier to form a complex due to the flexibility of the structure. The radius of gyration (R_g) was linked to the fluctuations in protein and ligand size. A larger R_g value indicated a loose packaging structure, whereas a lower R_g value indicated a more compact arrangement of the protein and ligand. Figure 15(c) depicts the R_g profile of the five models. In this figure, no significant fluctuation in the radius of gyration was observed. These findings suggested that no significant departure was seen, indicating that the models were in a stable condition. Figure 15(d) provides solvent-accessible surface areas (SASAs) of all models. This metric was determined in order to comprehend the variations in protein

https://doi.org/10.1021/acsomega.3c06379
ACS Omega 2023, 8, 44121−44138

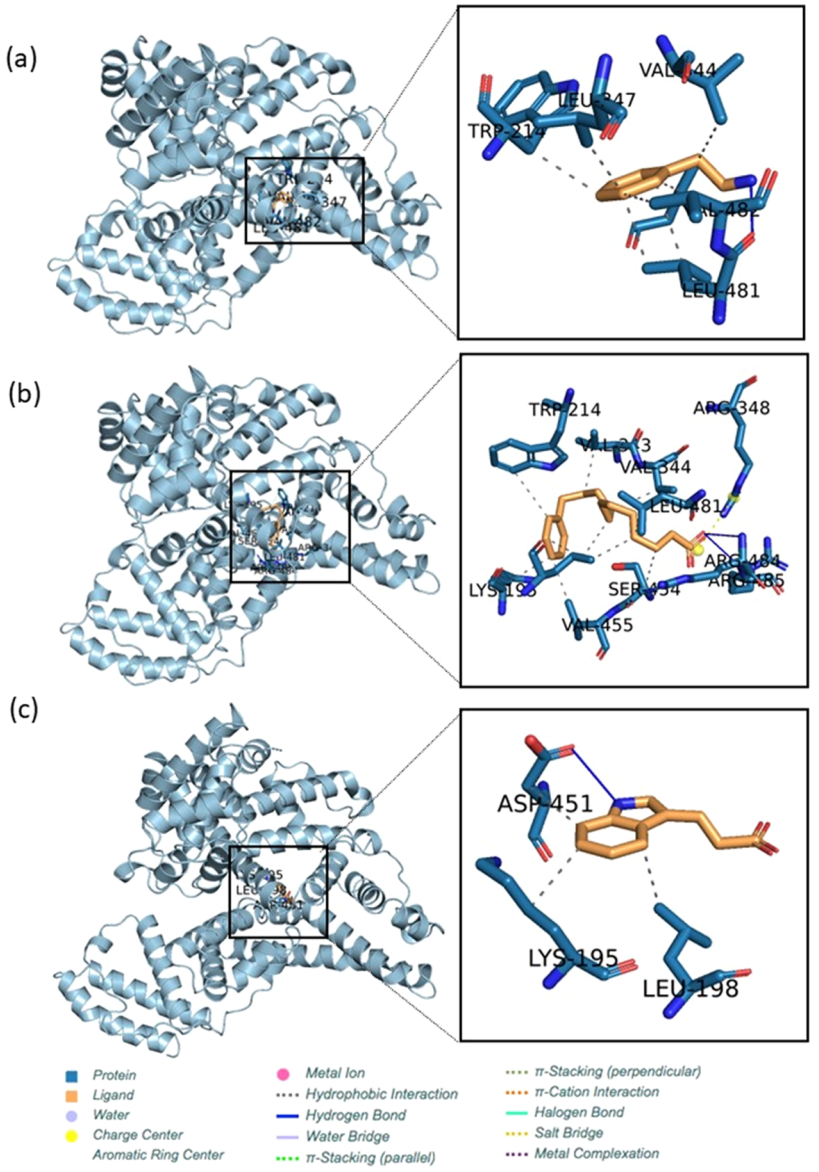

Figure 13. Conformational posture of the ligands to the protein target: (a) 2-phenylethanimine, (b) 12-phenyldodecanoic acid, and (c) indoleacrylic acid. The three dimensions (3D) of the model pocket are displayed using the PLIP online tool (https://plip-tool.biotec.tu-dresden.de/plip-web/plip/index) gathered with PyMOL v 2.3 software (https://pymol.org/2/).

volume for each model. As shown in this figure, all graphs showed similar trends until the end of the simulation. Overall, none of the models seemed to acquire volume during the simulation, and they all seemed to be stable structures. Moreover, the hydrogen-bond formation of each complex was also analyzed. This bond formation plays a crucial role in maintaining a biomolecular complex's stiffness. Figure 15(e) examines hydrogen bonding in an identical number ranging from 250 to 330. Our outcomes demonstrated that all models displayed comparable hydrogen profiles, indicating that their participation in the creation of hydrogen bonds helped maintain a stable complex throughout the simulation.

In the previous docking results listed in Table 4, the binding scores for all models show no significant difference in the binding energy values. Hence, the binding energies of all complexes were calculated using the MM-GBSA method based on the MD trajectories at the equilibrium phase. Table 8 lists the energy contributions for all complexes, including the control. The binding energies of models 1, 2, 3, 4, and 5 were −28.87, −67.90, −30.98, −58.99, and −21.59 kcal/mol, respectively. Each complex's ligands may be able to bind to ALB's catalytic site and potentially boost the protein activity, as shown by the fact that all models had a negative binding energy. Further, we observed that models 2 (12-phenyldodecanoic acid) and 4 (3,3-dimethyl-1-octadecyl-1,3-dihydrospiro[indole-2,3′-[1,4]oxazino[3,2-*f*]quinoline]) could be more stable structures because of the binding energy score, indicating that the strong binding of the ligand in complex with ALB might be found in ligands 2 and 4, followed by models 3 (indoleacrylic acid), 5 (4-aminobenzoic acid), and 1 (2-phenylethanimine). This result revealed that these active compounds might become supplementation ligands to activate the ALB to prevent stunted growth. Additionally, we noted that all of the contributions have considerably varied values, resulting in an impact on the complex's binding energy. These different contributions might be connected to the ligand's chemical structure, which affects the binding energy differently.

https://doi.org/10.1021/acsomega.3c06379
ACS Omega 2023, 8, 44121−44138

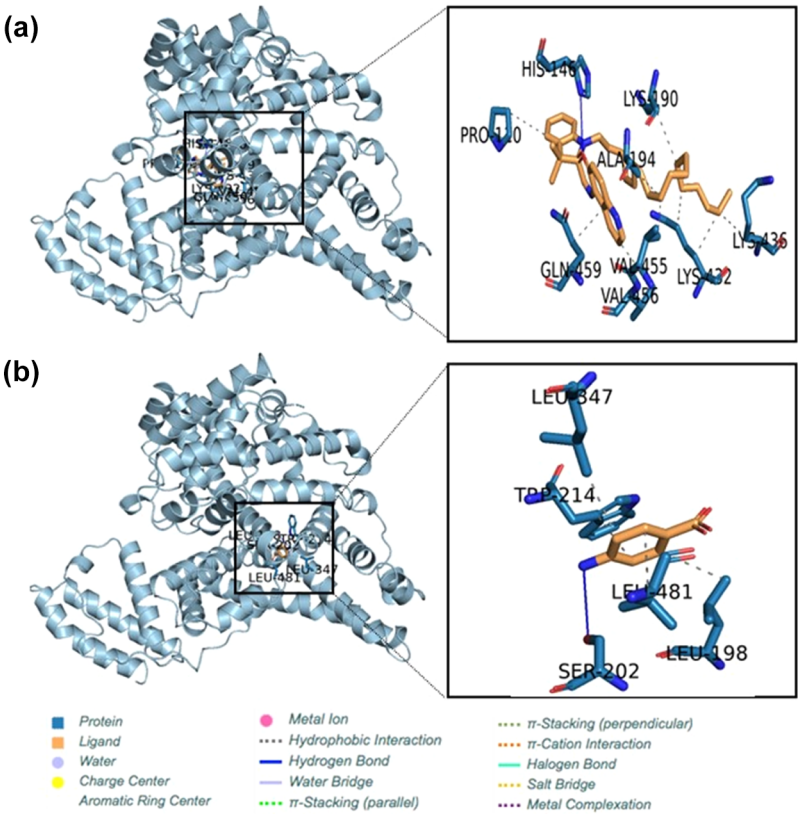

Figure 14. Conformational posture of the ligands to the receptor. (d) 3,3-Dimethyl-1-octadecyl-1,3-dihydrospiro[indole-2,3′-[1,4]oxazino[3,2-*f*]quinoline] and (e) 4-aminobenzoic acid. The three dimensions (3D) of the model pocket are displayed using the PLIP online tool (https://plip-tool.biotec.tu-dresden.de/plip-web/plip/index) gathered with PyMOL v 2.3 software (https://pymol.org/2/).

Table 5. Hydrogen Bonds of the Selected Compounds in Complex with the Receptor (ALB)

compound	residues	AA	distance H−A	distance D−A	donor angle	donor atom	acceptor atom
2-phenylethanimine	481A	LEU	2.43	2.93	108.91	5766 [N3]	4755 [O2]
12-phenyldodecanoic acid	484A	ARG	3.31	3.66	107.6	4780 [Nam]	5768 [O.co2]
	485A	ARG	2.33	3.19	174.33	4797 [Nam]	5768 [O.co2]
indoleacrylic acid	451A	ASP	2.36	3.08	126.75	5759 [Npl]	4453 [O.co2]
3,3-dimethyl-1-octadecyl-1,3-dihydrospiro[indole-2,3′-[1,4] oxazino[3,2-*f*]quinoline]	146A	HIS	3.39	3.78	104.87	1437 [Npl]	5759 [O3]
4-aminobenzoic acid	202A	SER	3.74	4.07	102.19	5765 [Npl]	1991 [O3]

DISCUSSIONS

Stunting has been identified as one of the main indicators of malnutrition in children. This indicates that a child has not grown to its full potential as a result of illnesses, poor health, and a lack of food. Millions of children worldwide also suffer from severe irreversible physical and intellectual impairment that comes along with stunted growth.[51] In societies where short height is prevalent, it is thought to be normal. Families and health professionals frequently fail to notice juvenile stunting. This is largely due to a lack of understanding of the severe health effects of stunting, as well as the fact that linear growth is not frequently assessed as part of community health programs. A child's linear growth must be assessed in order to determine whether they are developing normally or whether they have a growth problem or a propensity toward one that needs to be treated.[51,52]

Indonesia ranks third among countries with the highest prevalence of stunting in the Southeast Asia/Southeast Asia Regional (SEAR) region. The average prevalence of stunting from 2005 to 2017 for children under five years old was around 36.4%.[1,2] Thus, the government, stakeholders, and even the community must work together to address this issue by focusing on children's growth, their health, and even their adequate daily nutritional needs. At present, traditional plants are widely used in the prevention of stunted growth since it is believed that they contain medicinal components that can prevent or even treat many diseases. One common plant that Indonesians use to treat several ailments is *M. oleifera*. Pregnant and breastfeeding moms consume *M. oleifera* as a supplement to prevent stunted growth in their children.[53,54] However, the active compounds and molecular action of the plant in preventing stunting are not well-understood. Hence, molecular investigation utilizing a network pharmacology

https://doi.org/10.1021/acsomega.3c06379
ACS Omega 2023, 8, 44121−44138

Table 6. Hydrophobic Interaction of the Selected Compounds in Binding with the Receptor (ALB)

compound	residue	A–A	distance	ligand atom	protein atom
2-phenylethanimine	198A	LEU	3.78	5761	1944
	198A	LEU	3.76	5765	1946
	214A	TRP	3.57	5764	2132
	344A	VAL	3.9	5765	3402
	347A	LEU	3.2	5762	3429
	481A	LEU	3.49	5762	4759
	481A	LEU	3.64	5760	4757
	482A	VAL	3.75	5762	4766
12-phenyldodecanoic acid	195A	LYS	3.65	5779	1902
	198A	LEU	3.43	5777	1946
	198A	LEU	3.61	5759	1946
	198A	LEU	3.32	5763	1945
	214A	TRP	3.91	5775	2139
	343A	VAL	3.26	5772	3392
	344A	VAL	3.52	5770	3400
	454A	SER	3.85	5764	4481
	455A	VAL	3.23	5779	4500
	481A	LEU	3.58	5763	4757
indoleacrylic acid	195A	LYS	3.79	5767	1902
	198A	LEU	3.51	5764	1946
	451A	ASP	3.74	5765	4451
3,3-dimethyl-1-octadecyl-1,3-dihydrospiro[indole-2,3′-[1,4]oxazino[3,2-*f*] quinoline]	110A	PRO	3.97	5770	1060
	190A	LYS	3.73	5795	1860
	194A	ALA	3.66	5791	1895
	432A	LYS	3.73	5796	4265
	432A	LYS	3.56	5799	4263
	436A	LYS	3.61	5799	4305
	455A	VAL	3.9	5791	4501
	456A	VAL	4	5781	4510
	459A	GLN	3.65	5777	4537
4-aminobenzoic acid	198A	LEU	3.67	5762	1946
	214A	TRP	3.89	5764	2133
	347A	LEU	3.42	5763	3429
	481A	LEU	3.81	5761	4757

method shared with several computational approaches is employed to gain insight into the molecular action of the active compound in human growth.

The implementation of network pharmacology to explore the potency of the natural compound has been performed by a few research teams.[55−57] Network pharmacology was used by Sakle and co-workers to look into the possible targets of *Caesalpinia pulcherima*.[55] The authors suggested that four active compounds from the plant are potential drugs in breast cancer treatment. In the paper presented by Wu et al., the authors used a network pharmacology model to investigate the molecular action of *Uncaria* alkaloids against Alzheimer's disease and hypertension.[56] The main mechanisms of the antihypertensive effects of Uncaria alkaloids have been shown by the authors, and they also recognized a potential application for the potent chemicals in the treatment of Alzheimer's disease. YuPingFeng (YPF) granules are a classic herbal formula widely utilized in clinical practice in China against chronic obstructive pulmonary disease (COPD), which has been investigated by Yin and co-workers using network pharmacology analysis.[57] This finding suggested that the therapeutic effects of YPF in treating COPD might be contingent on the response to steroid hormones, glucocorticoids, and pathways connected to HIF-1 and apoptotic signaling. In this present investigation, network pharmacology was applied on the active compounds of *M. oleifera* leaves, exploring their potential as a food supplement for preventing stunting in children. 22 of 35 active compounds were identified in the PubChem database. Thus, we used those identified compounds for collecting the proteins using some databases such as TargetNet, SEA, and SwissTarget databases. 38 genes were found connecting *M. oleifera* and stunted growth. A protein−protein interaction (PPI) network was constructed, and the top three degrees of the topological network analysis were obtained corresponding to the proteins ALB, IL6, and EGFR. These proteins may be strongly associated with stunted growth.

The biological pathways of the obtained proteins related to human growth have been analyzed. Six pathways are identified and could be correlated to human growth, such as "Signaling of hepatocyte growth factor receptors", "Disease of signal transduction by growth factor receptors and second messengers", "Growth hormone receptor signaling", "Growth hormone signaling", "Growth hormone synthesis, secretion, and action", and "Mammary gland development pathway". Investigating these pathways is therefore essential to understanding the mechanisms underlying human growth. Further, in the previous network pharmacology investigation, 38 protein targets correlated with stunted growth were found. We selected only the first-degree rank (human serum albumin (ALB)) based on topological analysis as a receptor (human serum albumin) for molecular docking in order to shorten simulation times and lower computational costs. ALB is one of the components that is correlated with children's growth. In the paper presented by Sanaa and co-workers, the stunted growth of children was caused by a lack of nutrients such as vitamins A and K, carbohydrates, lipids, and hemoglobin, including human serum albumin.[58] Thus, it is interesting to investigate the molecular action of ALB in relation to human growth. Our docking results show that the selected ligands may

Table 7. Identity of MD Simulation for All Complexes

complex identities	identities			
	box size (Å)	no. of ions (Na^+)	no. of water	total atom
2-phenylethanimine	102.968 × 88.616 × 115.233	13	26,261	88,028
12-phenyldodecanoic acid	102.968 × 88.616 × 115.233	13	26,261	88,039
indoleacrylic acid	102.968 × 88.616 × 115.233	13	26,261	88,034
3,3-dimethyl-1-octadecyl-1,3-dihydrospiro[indole-2,3′-[1,4]oxazino[3,2-*f*] quinoline]	102.968 × 88.616 × 115.233	13	26,261	88,030
4-aminobenzoic acid	102.968 × 88.616 × 115.233	13	26,261	88,031

https://doi.org/10.1021/acsomega.3c06379
ACS Omega 2023, 8, 44121−44138

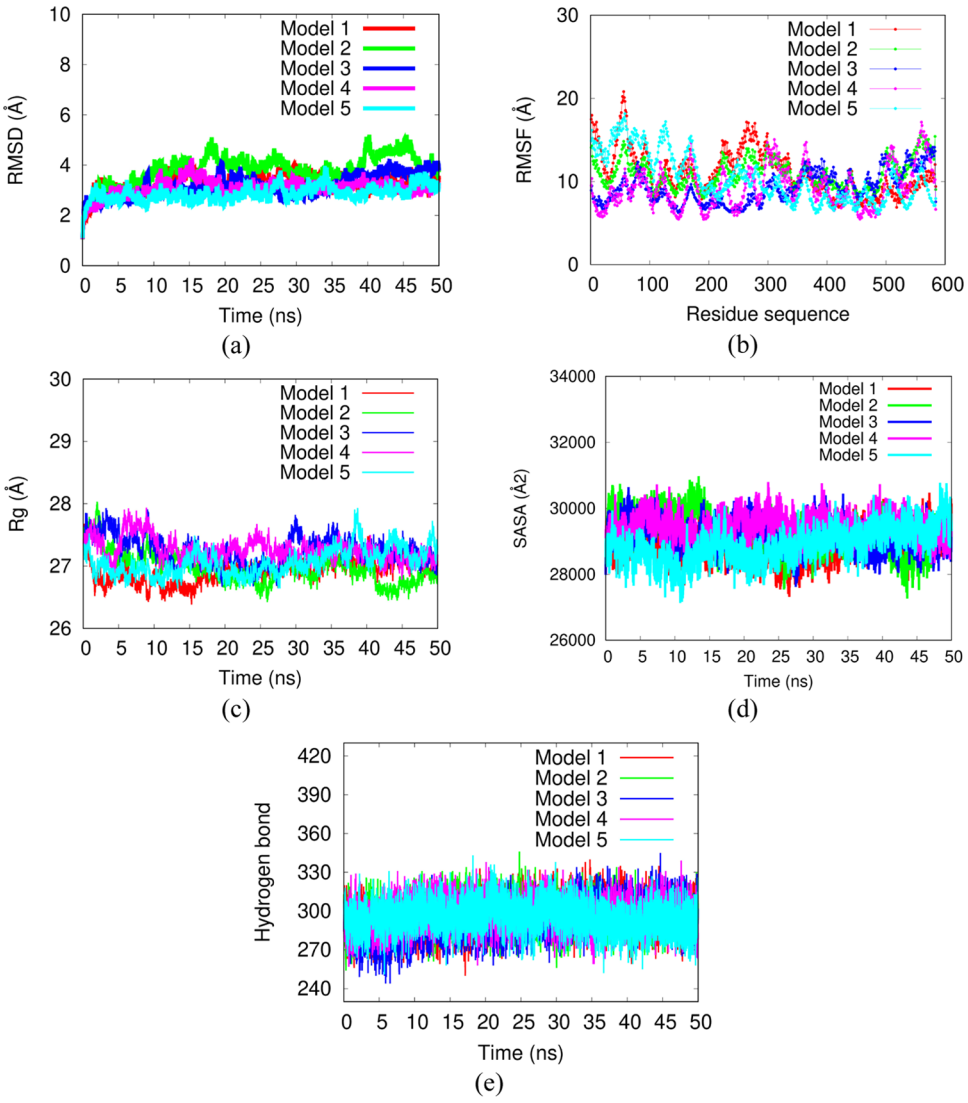

Figure 15. MD validation metrics consisting of the (a) RMSD value of the complexes, (b) RMSF descriptor, (c) R_g profile, (d) protein surface area measured from SASA, and (e) hydrogen bond calculated from MD trajectories. The ligand−receptor complexes corresponding to 2-phenylethanimine (Model 1), 12-phenyldodecanoic acid (Model 2), indoleacrylic acid (Model 3), 3,3-dimethyl-1-octadecyl-1,3-dihydrospiro-[indole-2,3′-[1,4]oxazino[3,2-*f*]quinoline] (Model 4), and 4-aminobenzoic acid (Model 5) are denoted by red, green, blue, magenta, and cyan colors, respectively.

Table 8. Contribution of Each Energy Term to the Binding Energy for All Models. All Energy Contributions Are Shown in kcal/mol Units[a]

model	E_{vdw}	E_{ele}	E_{GB}	E_{SA}	ΔG_{MM}	ΔG_{GBSA}	ΔG_{bind}
model 1	−28.96 (1.41)	−1.31 (0.87)	4.58 (0.48)	−3.17 (0.07)	−30.28 (1.60)	1.41 (0.47)	−28.87 (1.48)
model 2	−66.68 (2.27)	−5.81 (1.52)	11.38 (1.09)	−6.78 (0.10)	−72.50 (2.66)	4.59 (1.10)	−67.90 (2.22)
model 3	−34.59 (2.10)	−1.86 (1.58)	9.43 (1.37)	−3.95 (0.14)	−36.46 (2.54)	5.47 (1.37)	−30.98 (2.19)
model 4	−68.52 (3.94)	−2.06 (0.88)	18.59 (1.04)	−7.00 (0.33)	−70.58 (3.95)	11.59 (0.98)	−58.99 (4.00)
model 5	−24.39 (1.93)	−3.26 (1.93)	9.13 (1.40)	−3.07 (0.15)	−27.65 (2.85)	6.06 (1.34)	−21.59 (2.22)

[a]The standard deviation Is displayed in the parentheses.

attach to the receptors, indicating that they may form stable complexes. Additionally, each ligand formed hydrogen bonds and hydrophobic interactions with the critical ALB site,[31] showing that they might enhance ALB activity to prevent stunted growth. The stability of the complexes produced by molecular docking was assessed by using a range of MD validation metrics. Our findings showed that despite certain fluctuation points seen in some graphs, all models remained stable along the simulation, suggesting that all ligands could bind to the site of ALB to make a complex formation. Additionally, the MM-GBSA method was employed to calculate the binding energy for all models. Models 2 and 4 have a high energy score, suggesting that strong binding of the ligand in complex with ALB might be found in ligands 2 and 4, followed by models 3, 5, and 1. According to our findings,

https://doi.org/10.1021/acsomega.3c06379
ACS Omega 2023, 8, 44121−44138

ligands 2 and 4 could be useful as food supplements for the prevention of stunting.

CONCLUSIONS

In this research, we examined the active substances of *M. oleifera* as a potential food supplement for stunted growth prevention using network pharmacology and numerous in silico techniques. In network pharmacology, 38 crucial proteins are found that may have strong interconnections with stunted growth. To determine the pathways of those shared genes, 38 genes were submitted to several online platforms. Six pathways could be correlated to human growth, such as "Signaling of hepatocyte growth factor receptors", "Disease of signal transduction by growth factor receptors and second messengers", "Growth hormone receptor signaling", "Growth hormone signaling", "Growth hormone synthesis, secretion, and action", and "Mammary gland development pathway". Further, the top 5 active compounds identified by experimental research were used as ligands for molecular docking. Meanwhile, albumin protein (ALB) was used as a receptor based on the PPI topological analysis. From our docking results, all ligands bind to the receptors, suggesting that they could form stable complexes with the ALB protein. To confirm the stability of the ligand−receptor complex in the water solvent, MD simulations were performed. Our results implied that all models achieved a stable condition along the simulation based on the validation metrics such as RMSD, RMSF, R_g, SASA, and hydrogen bonds. Besides, the MM-GBSA method was employed to estimate the binding energy of five models. Models 2 and 4 have a high binding energy score, indicating that the strong binding of the ligand in complex with ALB might be found in ligands 2 and 4, followed by models 3, 5, and 1. Our results show that ligands 2 and 4 might become promising food supplements to prevent stunting in children.

ASSOCIATED CONTENT

Supporting Information

The Supporting Information is available free of charge at https://pubs.acs.org/doi/10.1021/acsomega.3c06379.

> Network of compound-target gene interactions connected with 22 active compounds of *Brucea javanica* and 603 target genes; PubChem ID and SMILE identities of the active compounds of *Moringa oleifera* obtained from PubChem Database; databases and software used (PDF)

AUTHOR INFORMATION

Corresponding Authors

Arwansyah Arwansyah − *Department of Chemistry Education, Faculty of Teacher Training and Education, Tadulako University, Palu 94148, Indonesia; Research Center for Genetic Engineering, National Research and Innovation Agency (BRIN), Bogor 16911, Indonesia;* orcid.org/0000-0003-1784-5942; Email: arwansyah@untad.ac.id

Abd Farid Lewa − *Department of Nutrition, Poltekkes Kemenkes Palu, Palu 94148, Indonesia*; Email: faridlewa75@gmail.com

Abdur Rahman Arif − *Department of Chemistry, Faculty of Mathematics and Natural Sciences, Hasanuddin University, Makassar 90245, Indonesia*; Email: arrahmanarif@unhas.ac.id

Authors

Muliani Muliani − *Department of Midwife, Poltekkes Kemenkes Palu, Palu 94148, Indonesia*

Siti Warnasih − *Department of Chemistry, Faculty of Mathematics and Natural Sciences, Pakuan University, Bogor 16129, Indonesia*

Apon Zaenal Mustopa − *Research Center for Genetic Engineering, National Research and Innovation Agency (BRIN), Bogor 16911, Indonesia*

Complete contact information is available at: https://pubs.acs.org/10.1021/acsomega.3c06379

Author Contributions

A.A., A.F.L., and A.R.A. planned the project, directed the research, examined both experimental and computational results, and wrote the original draft. M.M. and S.S. conducted the extraction process of *Moringa oleifera* leaves and validated the structural elucidation investigations of LC-MS results. A.Z.M. carried out data analysis and interpretation of in silico results and proofread the manuscript. All authors revised the manuscript and the Supporting Information.

Notes

The authors declare no competing financial interest.

ACKNOWLEDGMENTS

This research was supported by Poltekkes Kemenkes Palu in the form of providing raw materials and experimental analysis. The authors thank the National Research and Innovation Agency (BRIN) for providing computational resources.

REFERENCES

(1) Kemenkes.. *Hasil Survei Status Gizi Indonesia (SSGI) (Results of the 208 Indonesian Nutritional Status Survey (SSGI))*, 20181-7.

(2) WHO. World Health Statistics Data Visualizations Dashboard, 2023 https://apps.who.int/gho/data/node.sdg.2-2-viz-1?lang=en(2023).

(3) Media, I. Penyebab Prevalensi Stunting Masih Tinggi Di Indonesia (This Is the Cause of the High Prevalence of Stunting in Indonesia), 2023 https://mediaindonesia.com/humaniora/553355/ini-penyebab-prevalensi-stunting-masih-tinggi-di-indonesia.

(4) Muhammad, S. A.; Fatima, N. In Silico Analysis and Molecular Docking Studies of Potential Angiotensin-Converting Enzyme Inhibitor Using Quercetin Glycosides. *Pharmacogn. Mag.* **2015**, *11*, No. S123.

(5) Cahyaningsih, R.; Magos Brehm, J.; Maxted, N. Setting the Priority Medicinal Plants for Conservation in Indonesia. *Genet. Resour. Crop Evol.* **2021**, *68* (5), 2019−2050.

(6) Ghimire, S.; Subedi, L.; Acharya, N.; Gaire, B. P. *Moringa Oleifera*: A Tree of Life as a Promising Medicinal Plant for Neurodegenerative Diseases. *J. Agric. Food Chem.* **2021**, *69* (48), 14358−14371.

(7) Vergara-Jimenez, M.; Almatrafi, M. M.; Fernandez, M. L. Bioactive Components in *Moringa Oleifera* Leaves Protect against Chronic Disease. *Antioxidants* **2017**, *6* (4), No. 91.

(8) Kiranawati, T. M.; Nurjanah, N. Improvement of Noodles Recipe for Increasing Breastmilk: Design of the Moringa Noodles. *Am. J. Food Sci. Technol.* **2014**, *2* (3), 88−92.

(9) Fungtammasan, S.; Phupong, V. The Effect of *Moringa Oleifera* Capsule in Increasing Breastmilk Volume in Early Postpartum Patients: A Double-Blind, Randomized Controlled Trial. *PLoS One* **2021**, *16* (4), No. e0248950.

(10) Madjid, A.; Ramadanil, R. Ethnobotanical Study of "Kaili Inde Tribe" in Central Sulawesi Indonesia. *Emirates J. Food Agric.* **2016**, 337−347.

(11) Verma, A. K.; Rajkumar, V.; Kumar, M. S.; Jayant, S. K. Antioxidative Effect of Drumstick (*Moringa Oleifera* L.) Flower on the Quality and Stability of Goat Meat Nuggets. *Nutr. Food Sci.* **2019**, *50* (1), 84−95.
(12) Baxter, C. A.; Murray, C. W.; Waszkowycz, B.; Li, J.; Sykes, R. A.; Bone, R. G. A.; Perkins, T. D. J.; Wylie, W. New Approach to Molecular Docking and Its Application to Virtual Screening of Chemical Databases. *J. Chem. Inf. Comput. Sci.* **2000**, *40* (2), 254−262.
(13) Arwansyah, A.; Arif, A. R.; Ramli, I.; Hasrianti, H.; Kurniawan, I.; Ambarsari, L.; Sumaryada, T. I.; Taiyeb, M. Investigation of Active Compounds of Brucea Javanica In Treating Hypertension Using A Network Pharmacology-Based Analysis Combined with Homology Modeling, Molecular Docking and Molecular Dynamics Simulation. *ChemistrySelect* **2022**, *7* (1), No. e202102801.
(14) Rahmadani, K.; Manguntungi, B.; Arwansyah, A.; Jumadi, O.; Khizbullah, M. A.; Hidayat, A.; Ayunda, N. G. A.; Faiz, M.; Vanggy, L. R.; Septiawati, E. Efficiency of Nitrification Inhibitor on Designing Nitrogen Fertilizer by Neem Compounds Based on Molecular Docking. *Trends Sci.* **2023**, *20* (1), No. 6395.
(15) Natsir, H.; Arif, A. R.; Wahab, A. W.; Budi, P.; Arfah, R. A.; Arwansyah, A.; Fudholi, A.; Suriani, N. L.; Himawan, A.; et al. Inhibitory Effects of *Moringa Oleifera* Leaves Extract on Xanthine Oxidase Activity from Bovine Milk. *Pharmacia* **2022**, *69* (2), 363−375.
(16) Ismed, F.; Desti, W. N.; Arifa, N.; Rustini, R.; Putra, D. P. In*TLC-Bioautographic and LC-MS/MS Detection of Antimicrobial Compounds from Four Semipolar Extracts of Cladonia Species*, 2nd International Conference on Contemporary Science and Clinical Pharmacy 2021 (ICCSCP 2021); Atlantis Press, 2021; pp 49−59.
(17) Yao, Z.-J.; Dong, J.; Che, Y.-J.; Zhu, M.-F.; Wen, M.; Wang, N.-N.; Wang, S.; Lu, A.-P.; Cao, D.-S. TargetNet: A Web Service for Predicting Potential Drug−Target Interaction Profiling via Multi-Target SAR Models. *J. Comput.-Aided Mol. Des.* **2016**, *30* (5), 413−424.
(18) Gfeller, D.; Michielin, O.; Zoete, V. Shaping the Interaction Landscape of Bioactive Molecules. *Bioinformatics* **2013**, *29* (23), 3073−3079.
(19) Daina, A.; Michielin, O.; Zoete, V. SwissTargetPrediction: Updated Data and New Features for Efficient Prediction of Protein Targets of Small Molecules. *Nucleic Acids Res.* **2019**, *47* (W1), W357−W364.
(20) Szklarczyk, D.; Franceschini, A.; Wyder, S.; Forslund, K.; Heller, D.; Huerta-Cepas, J.; Simonovic, M.; Roth, A.; Santos, A.; Tsafou, K. P.; et al. STRING V10: Protein−Protein Interaction Networks, Integrated over the Tree of Life. *Nucleic Acids Res.* **2015**, *43* (D1), D447−D452.
(21) Szklarczyk, D.; Gable, A. L.; Lyon, D.; Junge, A.; Wyder, S.; Huerta-Cepas, J.; Simonovic, M.; Doncheva, N. T.; Morris, J. H.; Bork, P.; et al. STRING V11: Protein−Protein Association Networks with Increased Coverage, Supporting Functional Discovery in Genome-Wide Experimental Datasets. *Nucleic Acids Res.* **2019**, *47* (D1), D607−D613.
(22) Bindea, G.; Mlecnik, B.; Hackl, H.; Charoentong, P.; Tosolini, M.; Kirilovsky, A.; Fridman, W.-H.; Pagès, F.; Trajanoski, Z.; Galon, J. ClueGO: A Cytoscape Plug-in to Decipher Functionally Grouped Gene Ontology and Pathway Annotation Networks. *Bioinformatics* **2009**, *25* (8), 1091−1093.
(23) Wishart, D. S.; Knox, C.; Guo, A. C.; Cheng, D.; Shrivastava, S.; Tzur, D.; Gautam, B.; Hassanali, M. DrugBank: A Knowledgebase for Drugs, Drug Actions and Drug Targets. *Nucleic Acids Res.* **2008**, *36*, D901−D906.
(24) Shannon, P.; Markiel, A.; Ozier, O.; Baliga, N. S.; Wang, J. T.; Ramage, D.; Amin, N.; Schwikowski, B.; Ideker, T. Cytoscape: A Software Environment for Integrated Models of Biomolecular Interaction Networks. *Genome Res.* **2003**, *13* (11), 2498−2504.
(25) Zhou, Y.; Zhou, B.; Pache, L.; Chang, M.; Khodabakhshi, A. H.; Tanaseichuk, O.; Benner, C.; Chanda, S. K. Metascape Provides a Biologist-Oriented Resource for the Analysis of Systems-Level Datasets. *Nat. Commun.* **2019**, *10* (1), No. 1523.
(26) Liao, Y.; Wang, J.; Jaehnig, E. J.; Shi, Z.; Zhang, B. WebGestalt 2019: Gene Set Analysis Toolkit with Revamped UIs and APIs. *Nucleic Acids Res.* **2019**, *47* (W1), W199−W205.
(27) Kamburov, A.; Stelzl, U.; Lehrach, H.; Herwig, R. The ConsensusPathDB Interaction Database: 2013 Update. *Nucleic Acids Res.* **2013**, *41* (D1), D793−D800.
(28) Trott, O.; Olson, A. J. AutoDock Vina: Improving the Speed and Accuracy of Docking with a New Scoring Function, Efficient Optimization, and Multithreading. *J. Comput. Chem.* **2010**, *31* (2), 455−461.
(29) Kim, S.; Chen, J.; Cheng, T.; Gindulyte, A.; He, J.; He, S.; Li, Q.; Shoemaker, B. A.; Thiessen, P. A.; Yu, B.; et al. PubChem in 2021: New Data Content and Improved Web Interfaces. *Nucleic Acids Res.* **2021**, *49* (D1), D1388−D1395.
(30) O'Boyle, N. M.; Banck, M.; James, C. A.; Morley, C.; Vandermeersch, T.; Hutchison, G. R. Open Babel: An Open Chemical Toolbox. *J. Cheminf.* **2011**, *3* (1), No. 33.
(31) Johansson, E.; Nielsen, A. D.; Demuth, H.; Wiberg, C.; Schjødt, C. B.; Huang, T.; Chen, J.; Jensen, S.; Petersen, J.; Thygesen, P. Identification of Binding Sites on Human Serum Albumin for Somapacitan, a Long-Acting Growth Hormone Derivative. *Biochemistry* **2020**, *59* (14), 1410−1419.
(32) Morris, G. M.; Huey, R.; Lindstrom, W.; Sanner, M. F.; Belew, R. K.; Goodsell, D. S.; Olson, A. J. AutoDock4 and AutoDockTools4: Automated Docking with Selective Receptor Flexibility. *J. Comput. Chem.* **2009**, *30* (16), 2785−2791.
(33) Arwansyah, A.; Arif, A. R.; Kade, A.; Taiyeb, M.; Ramli, I.; Santoso, T.; Ningsih, P.; Natir, H.; Tahril, T.; Kumar, K. U. Molecular Modelling on Multiepitope-Based Vaccine Against SARS-CoV-2 Using Immunoinformatics, Molecular Docking, and Molecular Dynamics Simulation. *SAR QSAR Environ. Res.* **2022**, *33*, 649−675, DOI: 10.1080/1062936X.2022.2117846.
(34) Mustopa, A. Z.; Izaki, A. F.; Suharsono, S.; Fatimah, F.; Fauziyah, F.; Damarani, R.; Arwansyah, A.; Wahyudi, S. T.; Sari, S. S.; Rozirwan, R.; Bachtiar, Z. Characterization, Protein Modeling, and Molecular Docking of Factor C from Indonesian Horseshoe Crab (*Tachypleus Gigas*). *J. Genet. Eng. Biotechnol.* **2023**, *21* (1), No. 44.
(35) Arwansyah, A.; Arif, A. R.; Syahputra, G.; Sukarti, S.; Kurniawan, I. Theoretical Studies of Thiazolyl-Pyrazoline Derivatives as Promising Drugs against Malaria by QSAR Modelling Combined with Molecular Docking and Molecular Dynamics Simulation. *Mol. Simul.* **2021**, *47* (12), 988−1001.
(36) Salomon-Ferrer, R.; Case, D. A.; Walker, R. C. An Overview of the Amber Biomolecular Simulation Package. *WIREs Comput. Mol. Sci.* **2013**, *3*, 198.
(37) Jorgensen, W. L.; Chandrasekhar, J.; Madura, J. D.; Impey, R. W.; Klein, M. L. Comparison of Simple Potential Functions for Simulating Liquid Water. *J. Chem. Phys.* **1983**, *79* (2), 926−935.
(38) Wang, J.; Wolf, R. M.; Caldwell, J. W.; Kollman, P. A.; Case, D. A. Development and Testing a General Amber Force Field. *J. Comput. Chem.* **2004**, *25* (9), 1157−1174.
(39) Maier, J. A.; Martinez, C.; Kasavajhala, K.; Wickstrom, L.; Hauser, K. E.; Simmerling, C. Ff14SB: Improving the Accuracy of Protein Side Chain and Backbone Parameters from Ff99SB. *J. Chem. Theory Comput.* **2015**, *11* (8), 3696−3713.
(40) Essmann, U.; Perera, L.; Berkowitz, M. L.; Darden, T.; Lee, H.; Pedersen, L. G. A Smooth Particle Mesh Ewald Method. *J. Chem. Phys.* **1995**, *103* (19), 8577−8593.
(41) Ryckaert, J.-P.; Ciccotti, G.; Berendsen, H. J. C. Numerical Integration of the Cartesian Equations of Motion of a System with Constraints: Molecular Dynamics of n-Alkanes. *J. Comput. Phys.* **1977**, *23* (3), 327−341.
(42) Loncharich, R. J.; Brooks, B. R.; Pastor, R. W. Langevin Dynamics of Peptides: The Frictional Dependence of Isomerization Rates of N-Acetylalanyl-N-Methylamide. *Biopolymers* **1992**, *32* (5), 523−535.

(43) Roe, D. R.; Cheatham, T. E. PTRAJ and CPPTRAJ: Software for Processing and Analysis of Molecular Dynamics Trajectory Data. *J. Chem. Theory Comput.* **2013**, *9* (7), 3084−3095.
(44) Miller, B. R., III; McGee, T. D., Jr; Swails, J. M.; Homeyer, N.; Gohlke, H.; Roitberg, A. E. MMPBSA. Py: An Efficient Program for End-State Free Energy Calculations. *J. Chem. Theory Comput.* **2012**, *8* (9), 3314−3321.
(45) Jadhav, V.; Bhagare, A.; Wahab, S.; Lokhande, D.; Vaidya, C.; Dhayagude, A.; Khalid, M.; Aher, J.; Mezni, A.; Dutta, M. Green Synthesized Calcium Oxide Nanoparticles (CaO NPs) Using Leaves Aqueous Extract of *Moringa Oleifera* and Evaluation of Their Antibacterial Activities. *J. Nanomater.* **2022**, *2022*, No. 9047507.
(46) Sathasivam, T.; Hu, L.; Sugiarto, S.; Dou, Q.; Zhang, Z.; Ru Tan, H.; Leow, Y.; Zhu, Q.; Ken Lee, C.; Yu, H. Facile Fabrication of Lignin-Cellulose Green Nanogels. *Chem. - Asian J.* **2022**, *17* (21), No. e202200671.
(47) Sarkar, N.; Sharma, R. S.; Kaushik, M. Innovative Application of Facile Single Pot Green Synthesized CuO and CuO@ APTES Nanoparticles in Nanopriming of Vigna Radiata Seeds. *Environ. Sci. Pollut. Res.* **2021**, *28* (11), 13221−13228.
(48) Akbar, N.; Kawish, M.; Jabri, T.; Khan, N. A.; Shah, M. R.; Siddiqui, R. Cinnamic Acid and Lactobionic Acid Based Nano-formulations as a Potential Antiamoebic Therapeutics. *Exp. Parasitol.* **2023**, *246*, No. 108474.
(49) Rizwana, H.; Bokahri, N. A.; Alsahli, S. A.; Showiman, A. S. A.; Alzahrani, R. M.; Aldehaish, H. A. Postharvest Disease Management of Alternaria Spots on Tomato Fruit by *Annona Muricata* Fruit Extracts. *Saudi J. Biol. Sci.* **2021**, *28* (4), 2236−2244.
(50) Nasrollahzadeh, M.; Maham, M.; Rostami-Vartooni, A.; Bagherzadeh, M.; Sajadi, S. M. Barberry Fruit Extract Assisted in Situ Green Synthesis of Cu Nanoparticles Supported on a Reduced Graphene Oxide−Fe 3 O 4 Nanocomposite as a Magnetically Separable and Reusable Catalyst for the O-Arylation of Phenols with Aryl Halides under Ligand-Free C. *RSC Adv.* **2015**, *5* (79), 64769−64780.
(51) De Onis, M.; Branca, F. Childhood Stunting: A Global Perspective. *Matern. Child Nutr.* **2016**, *12*, 12−26.
(52) Balla, S.; Goli, S.; Vedantam, S.; Rammohan, A. Progress in Child Stunting across the World from 1990 to 2015: Testing the Global Convergence Hypothesis. *Public Health Nutr.* **2021**, *24* (17), 5598−5607.
(53) Veterini, A. S.; Susanti, E.; Ardiana, M.; Adi, A. C.; Rachmawati, H. Effects Of Consuming Biscuits Made From *Moringa Oleifera* Leaf On Body Weight And Height Of Children Under Five In Bangkalan, Madura Island. *Natl. Nutr. J./Media Gizi Indones.* **2023**, *18* (2), 150−156.
(54) Widowati, H.; Budiandari, R. U.; Hanum, S. M. F.; Sukarno, K. The Chemical Characteristic of Moringa Leaf Snack (*Moringa Oleifera*) as a Functional Food to Prevent Stunting *Academia Open* 2023; Vol. *8* (2), 6−12.
(55) Sakle, N. S.; More, S. A.; Mokale, S. N. A Network Pharmacology-Based Approach to Explore Potential Targets of Caesalpinia Pulcherima: An Updated Prototype in Drug Discovery. *Sci. Rep.* **2020**, *10* (1), No. 17217.
(56) Wu, W.; Zhang, Z.; Li, F.; Deng, Y.; Lei, M.; Long, H.; Hou, J.; Wu, W. A Network-Based Approach to Explore the Mechanisms of Uncaria Alkaloids in Treating Hypertension and Alleviating Alzheimer's Disease. *Int. J. Mol. Sci.* **2020**, *21* (5), No. 1766.
(57) Yin, Y.; Liu, J.; Zhang, M.; Li, R.; Liu, X.; Yang, Y.; Qu, Y.-Q. Mechanism of YuPingFeng in the Treatment of COPD Based on Network Pharmacology. *BioMed Res. Int.* **2020**, *2020*, No. 1630102, DOI: 10.1155/2020/1630102.
(58) Shaaban, S. Y.; Marzouk, D.; Nassar, M. F.; Ezzat, N. I.; Mohamed, I. Early Detection of Protein Energy Malnutrition in Sharkia Governorate. *J. Egypt. Public Health Assoc.* **2005**, *80* (5−6), 665−685.

https://doi.org/10.1021/acsomega.3c06379
ACS Omega 2023, 8, 44121−44138